

Official Journal of Turkish Society of Magnetic Resonance

# CRMRI

## Current Research in MRI

**Susceptibility-Weighted Imaging Features of Meningiomas with Histopathologic Correlation**  
Onur Taydaş, Ali Köksal, Hayri Oğul

**Can We Predict Triple Negative Breast Cancer with Magnetic Resonance Imaging Findings?**  
Eda Cingöz, Rana Günöz Cömert, Zuhale Bayramoğlu, Neslihan Cabioğlu, Ravza Yılmaz

**The Relationship Between Dorsal Subcutaneous Fat Tissue Thickness and Lumbar Disc Herniation: A Magnetic Resonance Imaging-Based Study**  
Volkan Kızılgöz

**Is Fusion Imaging Mandatory to Detect the Localization of Middle Ear Cholesteatomas? Inter-rater Reliability in Assessment**  
Umut Perçem Orhan Söylemez, Başak Atalay, Nesrin Gündüz, Sabriye Gülçin Bozbeyoğlu, Ali Fırat

# Current Research in MRI

## Editor in Chief

**Mecit Kantarcı** 

Department of Radiology, Erzincan Binali Yıldırım University, Faculty of Medicine; Atatürk University, Faculty of Medicine, Erzincan, Erzurum, Turkey

## Editors

### Abdominal Radiology

**Aytekin Oto** 

The University of Chicago, Department of Radiology, Chief Physician, Head of the Faculty Practice Plan and Dean for Clinical Affairs, Chicago, USA

**Murat Danacı** 

Department of Radiology, Ondokuz Mayıs University, Faculty of Medicine, Samsun, Turkey

### Breast Radiology

**Serap Gültekin** 

Department of Radiology, Gazi University, Faculty of Medicine, Ankara, Turkey

### Cardiac Radiology

**Memduh Dursun** 

Department of Radiology, İstanbul University, İstanbul Faculty of Medicine, İstanbul, Turkey

**Cihan Duran** 

Department of Diagnostic and Interventional Imaging, The University of Texas, McGovern Medical School, Texas, USA

### Emergency Radiology

**Mehmet Ruhi Onur** 

Department of Radiology, Hacettepe University Faculty of Medicine Hospital, Ankara, Turkey

### Engineer Group

**Esin Öztürk Işık** 

Biomedical Engineering, Boğaziçi University, İstanbul, Turkey

### Head & Neck Radiology

**Nafi Aygün** 

Department of Radiology, Johns Hopkins University School of Medicine, Baltimore, Maryland, USA

**Hatice Gül Hatipoğlu** 

Department of Radiology, Health Science University, Gulhane Faculty of Medicine, Ankara Bilkent City Hospital, Ankara, Turkey

### Musculoskeletal Radiology

**Nil Tokgöz** 

Department of Radiology, Gazi University, Faculty of Medicine, Ankara, Turkey

### Neuroradiology Radiology


**Alpay Alkan** 

Department of Radiology, Bezmialem Vakıf University, Faculty of Medicine, İstanbul, Turkey

### Pediatric Radiology

**Korgün Koral** 

Department of Radiology, University of Texas Southwestern Medical Center, Dallas, TX, USA

**Süreyya Burcu Görkem** 

Department of Pediatric Radiology, Adana State Hospital, Adana, Turkey

### Thorax Radiology

**Polat Koşucu** 

Department of Radiology, Karadeniz Teknik University, Faculty of Medicine, Trabzon, Turkey

### Biostatistical Consultant

**Sonay Aydın** 

Department of Radiology, Erzincan Binali Yıldırım University, Faculty of Medicine, Erzincan, Turkey

Türk Manteyik Rezonans Derneği adına sahibi / Owner: Abdülmecit Kantarcı • Sorumlu Yazı İşleri Müdürü / Responsible Manager on behalf of the Turkish Society of Magnetic Resonance: Sonay Aydın • Yayın türü / Publication Type: Yerel süreli / Local periodical • Basım yeri / Printed at: Kaya Ozalit, Meclis-i Mebusan cad. Mimar Han No:75/A 34427 Fındıklı İstanbul, Turkey (+90 212 243 81 05) • Basım tarihi / Printing Date: Ağustos 2022 / August 2022 • Türk Manteyik Rezonans Derneği tarafından yayınlanmaktadır / Published by Turkish Society of Magnetic Resonance, Konak Mah. 858. Sok. No:2 Çakıroğlu İş Hanı Kat:5 Daire:55 Konak / İzmir (+90 232 446 75 96)



#### Founder

İbrahim KARA

#### General Manager

Ali ŞAHİN

#### Publishing Directors

İrem SOYSAL

Gökhan ÇİMEN

#### Editor

Bahar ALBAYRAK

#### Publications Coordinators

Arzu ARI

Deniz KAYA

İrmak BERBEROĞLU

Alara ERGİN

Hira Gizem FIDAN

Vuslat TAŞ

İrem ÖZMEN

#### Web Coordinators

Sinem Fehime KOZ

Doğan ORUÇ

#### Finance Coordinator

Elif YILDIZ ÇELİK

#### Contact

Address: Büyükdere Cad. No: 105/9

34394 Mecidiyeköy, Şişli-İstanbul

Phone: +90 212 217 17 00

E-mail: info@avesyayincilik.com

## AIMS AND SCOPE

Current Research in MRI (Curr Res MRI) is a scientific, open access, online-only official publication of the Turkish Society of Magnetic Resonance published in accordance with independent, unbiased, and double-blinded peer-review principles. The journal is published triannually in April, August, and December. The publication language of the journal is English.

Current Research in MRI aims to contribute to the literature by publishing manuscripts at the highest scientific level on radiology. The journal publishes original articles, reviews, case reports, and letters to the editor that are prepared in accordance with ethical guidelines.

The target audience of the journal includes specialists, researchers and professionals who working and interested in the field of radiology.

The editorial and publication processes of the journal are shaped in accordance with the guidelines of the International Committee of Medical Journal Editors (ICMJE), World Association of Medical Editors (WAME), Council of Science Editors (CSE), Committee on Publication Ethics (COPE), European Association of Science Editors (EASE), and National Information Standards Organization (NISO). The journal is in conformity with the Principles of Transparency and Best Practice in Scholarly Publishing (doaj.org/bestpractice).

### Publication Fee Policy

All expenses of the journal are covered by the Turkish Society of Magnetic Resonance. Processing and publication are free of charge with the journal. No fees are requested from the authors at any point throughout the evaluation and publication process. All manuscripts must be submitted via the online submission system, which is available at <http://curremr.com>. The journal guidelines, technical information, and the required forms are available on the journal's web page.

### Advertisement Policy

Current Research in MRI can publish advertisement images in the journal's website upon the approval of the Editor in

Chief. Potential advertisers should contact the Editorial Office. Advertisers have no effect on the editorial decisions or advertising policies.

### Disclaimer

Statements or opinions expressed in the manuscripts published in the journal reflect the views of the author(s) and not the opinions of the editors, editorial board, and/or publisher; the editors, editorial board, and publisher disclaim any responsibility or liability for such materials.

### Open Access Statement

Current Research in MRI is an open access publication, and the journal's publication model is based on Budapest Access Initiative (BOAI) declaration. All published content is available online, free of charge at <http://curremr.com>. The journal's content is licensed under a Creative Commons Attribution-NonCommercial (CC BY-NC) 4.0 International License which permits third parties to share and adapt the content for non-commercial purposes by giving the appropriate credit to the original work.

You can reach the current version of the instructions to authors at <https://curremr.com/EN>

**Editor in Chief: Mecit Kantarcı**

**Address:** Department of Radiology, Erzincan Binali Yıldırım University School of Medicine, Erzincan, Turkey

**E-mail:** [akkanrad@hotmail.com](mailto:akkanrad@hotmail.com)

**Publisher: Turkish Society of Magnetic Resonance**

**Address:** Konak Mah. 858. Sok. No: 2 Çakıroğlu İş Hanı Kat: 5 Daire: 55 Konak / İzmir, Turkey

**Publishing Service: AVES**

**Address:** Büyükdere Cad., 105/9 34394 Şişli, İstanbul, Turkey

**Phone:** +90 212 217 17 00

**E-mail:** [info@avesyayincilik.com](mailto:info@avesyayincilik.com)

**Webpage:** [www.avesyayincilik.com](http://www.avesyayincilik.com)



## CONTENTS

### REVIEW ARTICLE

- 24 Magnetic Resonance Imaging Findings in Mayer–Rokitansky–Kuster–Hauser Syndrome: A Review Article  
Özlem Kadirhan, Erdem Fatihoglu

### ORIGINAL ARTICLES

- 27 Susceptibility-Weighted Imaging Features of Meningiomas with Histopathologic Correlation  
Onur Taydaş, Ali Köksal, Hayri Oğul
- 33 Can We Predict Triple Negative Breast Cancer with Magnetic Resonance Imaging Findings?  
Eda Cingöz, Rana Günöz Cömert, Zuhale Bayramoğlu, Neslihan Cabioğlu, Ravza Yılmaz
- 38 The Relationship Between Dorsal Subcutaneous Fat Tissue Thickness and Lumbar Disc Herniation: A Magnetic Resonance Imaging-Based Study  
Volkan Kızılgöz
- 42 Is Fusion Imaging Mandatory to Detect the Localization of Middle Ear Cholesteatomas? Inter-rater Reliability in Assessment  
Umut Perçem Orhan Söylemez, Başak Atalay, Nesrin Gündüz, Sabriye Gülçin Bozbeyoğlu, Ali Fırat

### CASE REPORTS

- 47 Acute Transverse Myelitis in a Child with Down Syndrome After Pfizer-BioNTech COVID-19 Vaccine Second Dose  
Esra Sarıgeçili, Ümit Çelik, Okan Dilek, Ulaş Özdemir
- 50 Magnetic Resonance Imaging Findings in Osgood Schlatter Disease: A Case Report  
Özlem Kadirhan, Erdem Fatihoglu



# Magnetic Resonance Imaging Findings in Mayer–Rokitansky–Kuster–Hauser Syndrome: A Review Article

Özlem Kadirhan<sup>1</sup>, Erdem Fatihoğlu<sup>2</sup>

Department of Radiology, Erzincan University, Faculty of Medicine, Erzincan, Turkey

**Cite this article as:** Kadirhan Ö, Fatihoğlu E. Magnetic resonance imaging findings in Mayer–Rokitansky–Kuster–Hauser syndrome: A review article. *Current Research in MRI*. 2022; 1(2): 24-26.

**Corresponding author:** Özlem Kadirhan, e-mail: ozlemkkadirhan@gmail.com

**Received:** July 24, 2022 **Accepted:** September 16, 2022

DOI:10.5152/CurrResMRI.2022.221117



Content of this journal is licensed under a Creative Commons Attribution-NonCommercial 4.0 International License.

## Abstract

Mayer–Rokitansky–Kuster–Hauser syndrome is a congenital disorder characterized by uterine aplasia and upper vaginal aplasia in women with normal secondary sex characteristics and a normal female karyotype. Patients often present to the hospital with the complaint of primary amenorrhea in the presence of normal pubertal development and secondary sexual characteristics in adolescence. It is stated that the frequency is approximately 1 in every 5000 live female births. In recent years, neovagina and infertility treatment options have been increasing in the management of these patients. The use of imaging has made the diagnosis and evaluation of this disease much more efficient. This study aimed to highlight the findings of magnetic resonance due to its high efficiency in diagnosing and managing Mayer–Rokitansky–Kuster–Hauser syndrome as it is a non-invasive method.

**Keywords:** MRKH, mullerian agenesis, uterovaginal agenesis, infertility, neovagina

## INTRODUCTION

The Mayer–Rokitansky–Kuster–Hauser (MRKH) syndrome is a condition characterized by congenital aplasia or severe hypoplasia of the uterus, upper vagina, and fallopian tubes, which are tissues originating from the Müllerian duct. It has been found to occur in 1 out of every 4000-5000 newborns.<sup>1</sup> It manifests itself with primary amenorrhea in the presence of normal pubertal development and secondary sexual characteristics due to the normal functioning of the ovaries in adolescent patients. In young women, the MRKH condition has disastrous consequences for fertility and sexual intercourse.

To facilitate clinical and psychologic input, it is critical that the diagnosis be made swiftly and precisely. Despite the fact that magnetic resonance (MR) imaging is widely accepted as a valuable modality, there are few publications in the literature, and they focus on a small number of women.<sup>2</sup> There are little precise descriptions of what to expect in these conditions. It is a widely known misconception that there is no uterine development in patients with MRKH syndrome; consequently, if primitive Mullerian structures are present, diagnostic confusion may arise.<sup>3</sup> Although ultrasonography is the first step in imaging methods, the main role in the diagnosis of patients belongs to MR examination.

## History, Embryology, Etiology, and Genetics

This syndrome was named after the research carried out by the German anatomist August Franz Josef Karl Mayer (1829), the Austrian anatomist Carl von Rokitansky (1838), the German gynecologist Hermann Küster (1910), and the Swiss gynecologist Georges Andre Hauser (1961). Years later, Küster was the first to report this case by removing the painful uterine remnant. Hauser and Schreiner described uterovaginal agenesis in 21 cases with normal karyotype and normal genotype. Schmid-Tannwald and Hauser showed that extragenital findings can be added to uterovaginal agenesis. In this way, type 2 classification has emerged in the current literature. Type 1 MRKH is 56%-72%, and no additional findings are observed. Type 2 MRKH is seen at a rate of 28%-44% and has extragenital findings (such as renal and musculoskeletal systems).<sup>4</sup>

The female reproductive system in humans includes the fallopian tubes, uterus, cervix, and vagina. The paramesonephric ducts (PMDs) are the source of the upper two-thirds of the vagina, the cervix, the uterus, and the fallopian tube, while the urogenital sinus is the source of the lower third of the vagina. The uterus, cervix, and upper vagina are formed by fusing the caudal parts of the 2 PMDs, whereas the oviducts are formed from the upper part of the PMD on the side. Mayer–Rokitansky–Kuster–Hauser syndrome is caused by a state of complete agenesis or partial aplasia of PMDs that make up the uterus and upper vaginal wall.<sup>5,6</sup>

Many genetic and environmental factors are considered in the etiology. Based on developmental pathways and linked illnesses, several other potential genes have been disproven to cause MRKH syndrome.<sup>4</sup> The presence of WNT4 mutations has been detected in patients with Müllerian aplasia and virilization. This, however, should be seen as a distinct entity rather than a cause of MRKH syndrome. In addition, it has been discovered that there are genetic polymorphisms in the WNT9B gene, which plays a role in the development of the genitourinary system and acts upstream of

WNT4. A recent study investigating male microchimerism as a possible cause failed to obtain sufficient data to support this conclusion.<sup>7,8</sup>

### Clinical Presentation and First Imaging Methods

The most common early MRKH symptoms are primary amenorrhea in a healthy adolescent female. When physical examination results consistent with an incomplete or hypoplastic vagina are obtained, MRKH and complete androgen insensitivity syndrome caused by an inactivating mutation in the androgen receptor can be considered among the differential diagnoses. After MRKH is determined, imaging examinations are very important in determining the extent of abnormalities. Some studies have found that most patients have concomitant anomalies, mainly anomalies of the renal and skeletal systems. Renal agenesis was the most common concomitant renal anomaly.<sup>1,9</sup>

Ultrasound and magnetic resonance imaging are the 2 most common imaging studies. Ultrasound is inexpensive and easy to use, but it is not always successful in detecting underdeveloped Müllerian structures and ovaries of different localization. It has been found that the ovaries are outside the typical location in approximately 16%-19% of patients.<sup>10</sup> According to various studies, MRI is the preferred procedure for detecting uterine abnormalities, including MRKH.<sup>11</sup> According to studies, MRI and laparoscopic examinations are highly associated, and the majority of them are based on bilateral uterine examinations. In recent articles, it has been understood that MRI can adequately show the endometrial tissue in the rudimentary uterus. In addition, it has been found that MRI has sufficient diagnostic power compared to laparoscopy, which is an invasive method.<sup>1</sup> Briefly, previous research has demonstrated that MRI is 100% sensitive and specific in the diagnosis of MRKH syndrome when paired with other diagnostic methods such as ultrasonography or laparoscopy.<sup>12</sup> Accordingly, MRI is the most useful noninvasive method for surgical planning. Sample cases are shown in Figures 1-3.

### Magnetic Resonance Imaging Findings

There is no standard MRI protocol determined in the literature. Axial, coronal T1-weighted (T1W); axial, coronal, sagittal T2-weighted; and sometimes fat-printed T2-weighted (T2W) pelvic MRI images were produced using 1, 1.5, and 3 T multiplanar scanners. Three-dimensional SPACE arrays, gradient-required echo, and diffusion-weighted images were also used in some patients. Although intravenous contrast material was used during imaging in some of the patients, it was observed that imaging was performed without contrast material in some of them.<sup>13</sup> The presence and degree of development of the vaginal canal can be assessed by looking at the presence of a low-signal density structure



**Figure 1.** Thin rudimentary uterus is seen between bladder and rectum in postcontrast T1 sequence in the sagittal view (arrow).

between the urethra–bladder neck and rectum in sagittal and axial T2W and 3D SPACE images. In addition, T2W images of hypointense muscle and fibrous tunica may contrast with T2W images of hyperintense mucosa and mucus in the vaginal lumen.<sup>14</sup> T1-weighted and T2-weighted images should be used to evaluate the presence, location, volume, and differentiation of Müllerian buds into layers. On T1W images, uterine remnants may appear as an elongated or oval solid structure with isointense to low signal intensities. Potential cavitation within the uterine buds can be demonstrated by T2W images. The cavitation occurs as a target pattern with a center region of T2W hyperintense signal intensity indicating the endometrium, surrounded by intermediate signal intensity of the junctional zone and medium to high signal intensity of the muscle layer.<sup>15</sup> The ovaries showed isointense to hypointense signal intensity on T1W images and mixed signal intensity on T2W images with T2 hyperintense ovarian follicles and T2W low signal intensity ovarian stroma.<sup>16</sup> Because of the frequent association of MRKH syndrome with renal agenesis and pelvic renal ectopia, abdominal sequences are also obtained to evaluate the renal compartment in all cases.<sup>17</sup>

The perception in the literature that the uterus is completely agenetic is incorrect because most patients have a rudimentary uterus.<sup>11</sup> Hall-Craggs et al<sup>2</sup> showed the presence of a rudimentary uterus in 93% of

### MAIN POINTS

- Mayer–Rokitansky–Kuster–Hauser (MRKH) syndrome is characterized by congenital complete aplasia or severe hypoplasia of tissues originating from the müller duct.
- Since ovarian function is normal in MRKH, pubertal development and secondary sexual characteristics are normal, but primary amenorrhea is present due to Müllerian anomaly.
- More than half of the patients with MRKH are accompanied by gynecological or extragynecological anomalies, and ultrasound alone is insufficient to detect them.
- Magnetic resonance imaging is the most useful method for detecting underdeveloped Müllerian structures and ovaries and planning surgery.

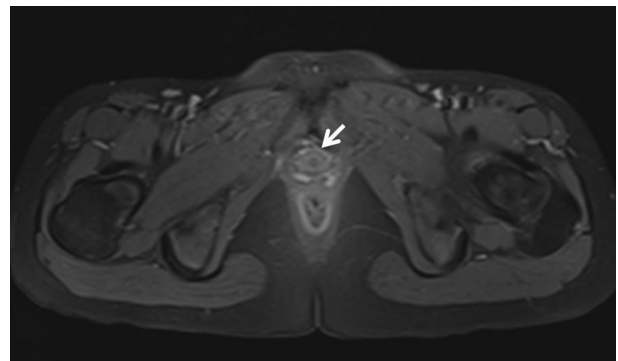


**Figure 2.** Presence of the distal vagina in the axial view in the post-contrast T1 sequence (arrow).

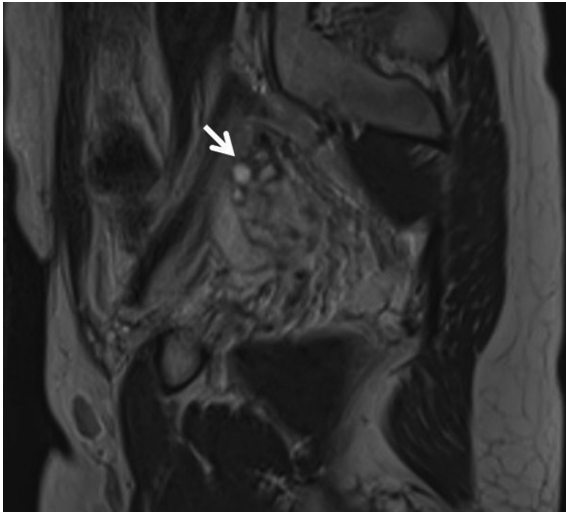


**Figure 3.** Presence of normal ovarian tissue in the unenhanced T2 sagittal image (arrow).

patients, similar to laparoscopy. However, although the uterine volume is large, it is understood that its parts such as fundus and ostium cannot be organized. The number of patients for whom these departments can be organized is quite limited. It has been shown that the rudimentary uterus is bilateral in 82%, unilateral in 11%, and agenetic in 8%. In most patients, it is located in the midline but only in the inferior caudal margin and laterally in only 1% of the population. In completely agenetic patients, a thin band with a low signal and difficulty to distinguish was noted in the uterine trace. In rare cases, the rudimentary uterus has also been shown to occur in the anterior ovary and inguinal canal. Even when the ovaries were ectopic, all uteri were instantly connected to the caudal edge of their matched ovary, and this association remained constant. Patients with MRKH syndrome may have a large primitive uterus (range, 0.4-80.2 mL) with an average volume of 6.4 mL, which can mimic a normal postpartum uterus. The primitive uterus in patients with MRKH syndrome has varying degrees of layer differentiation (8% are all uterine layers, 13% are 2-layer, 21% are single-layer).<sup>2</sup> It was noted that the rate of selection of the separation of the 3 layers increased in uteri with a volume greater than 20 mL. However, no matter how much the volume increased, the cervix could not be observed in the cases. In addition, it has been shown that the susceptibility to adenomyosis increases as the uterine volume increases in patients. In cases where the ovarian volume is more than 80 mL, blood products indicating that the endometrial tissue is functional were observed. Circular pelvic pain has also been shown to occur in these cases. The presence of bilateral ovarian tissue could be demonstrated in 95% of the patients. In cases where ovarian tissue could not be observed, the diagnosis of ectopic localization was considered as a priority, since there was normal sexual development and gonadotropin levels were sufficient. In the search for ectopic ovarian tissue, first of all, the pelvic anterior-lateral region, around the pelvic bone and around the anterior abdominal wall, should be carefully examined. The mean ovarian volume was observed to be around 10 mL. Vaginal length reaching an average of 2 cm was detected in 70% of the patients, while only vaginal dimple was observed in the remaining population.<sup>2,11</sup>

## CONCLUSION

Mayer-Rokitansky-Küster-Hauser syndrome is a congenital malformation of normal ovaries with agenesis of their tissues of

varying degrees of PMD origin, which may be accompanied by extra-gynecological abnormalities of varying degrees. Patients with MRKH are treated for neovagina formation or reproduction with newer assisted reproductive techniques. Magnetic resonance imaging is a noninvasive method that helps to provide better preoperative counseling in MRKH patients, and knowing its findings is important in diagnosis and treatment planning.

**Peer-review:** Externally peer-reviewed.

**Author Contributions:** Concept – O.K., E.F.; Design – O.K., E.F.; Supervision – O.K., E.F.; Fundings – None; Materials – O.K., E.F.; Data Collection and/or Processing – O.K., E.F.; Analysis and/or Interpretation – O.K., E.F.; Literature Review – O.K., E.F.; Writing – O.K., E.F.; Critical Review Contribution Type – O.K., E.F.

**Declaration of Interests:** The authors have no conflicts of interest to declare.

**Funding:** The authors declared that this study has received no financial support.

## REFERENCES

1. Londra L, Chuong FS, Kolp LJ. Mayer-Rokitansky-Kuster-Hauser Syndr Rev. *Int J Womens Health*. 2015;7:865.
2. Hall-Craggs MA, Williams CE, Pattison SH, Kirkham AP, Creighton SMJR. Mayer-Rokitansky-Kuster-Hauser syndrome: diagnosis with MR imaging. *Radiology*. 2013;269(3):787-792. [\[CrossRef\]](#)
3. Acién P, Acién M, Sánchez-Ferrer MJHR. Complex malformations of the female genital tract. New types and revision of classification. *Hum Reprod*. 2004;19(10):2377-2384. [\[CrossRef\]](#)
4. Herlin MK, Petersen MB, Brännström MJO. Mayer-Rokitansky-Küster-Hauser (MRKH) syndrome: a comprehensive update. *Orphanet J Rare Dis*. 2020;15(1):1-16.
5. Cunha GR, Robboy SJ, Kurita T, et al. Development of the human female reproductive tract. *Differentiation*. 2018;103:46-65. [\[CrossRef\]](#)
6. Kobayashi A, Behringer. *RRJNRG. Dev Genet Female Reprod Tract Mamm*. 2003;4(12):969-980.
7. Peters HE, Johnson BN, Ehli EA, et al. Low prevalence of male microchimerism in women with Mayer-Rokitansky-Küster-Hauser syndrome. *Hum Reprod*. 2019;34(6):1117-1125. [\[CrossRef\]](#)
8. Waschke DE, Tewes AC, Römer T, et al. Mutations in WNT9B are associated with Mayer-Rokitansky-Küster-Hauser syndrome. *Clin Genet*. 2016;89(5):590-596. [\[CrossRef\]](#)
9. Oppelt PG, Lermann J, Strick R, et al. Malformations in a cohort of 284 women with Mayer-Rokitansky-Küster-Hauser syndrome (MRKH). *Reprod Biol Endocrinol*. 2012;10(1):57. [\[CrossRef\]](#)
10. Fedele L, Bianchi S, Frontino G, Ciappina N, Fontana E, Borroto FJO. Laparoscopic findings and pelvic anatomy in Mayer-Rokitansky-Küster-Hauser syndrome. *Obstet Gynecol*. 2007;109(5):1111-1115. [\[CrossRef\]](#)
11. Pompili G, Munari A, Franceschelli G, et al. Magnetic resonance imaging in the preoperative assessment of Mayer-Rokitansky-Küster-Hauser syndrome. *Radiol Med*. 2009;114(5):811-826. [\[CrossRef\]](#)
12. Lermann J, Mueller A, Wiesinger E, et al. Comparison of different diagnostic procedures for the staging of malformations associated with Mayer-Rokitansky-Küster-Hauser syndrome. *Fertil Steril*. 2011;96(1):156-159. [\[CrossRef\]](#)
13. Bhayana A, Ghazi RGJT. MRI Evaluation of Pelvis in Mayer-Rokitansky-Küster-Hauser Syndrome: Interobserver Agreement for Surgically Relevant Structures. *Bjor*. 2019;92(1097):20190045.
14. Siegelman ES, Outwater EK, Banner MP, Ramchandani P, Anderson TL, Schnall MDJR. High-resolution MR imaging of the vagina. *Radiographics*. 1997;17(5):1183-1203. [\[CrossRef\]](#)
15. Saleem SNJR. MR imaging diagnosis of uterovaginal anomalies: current state of the art. *RadioGraphics*. 2003;23(5):e13-e13. [\[CrossRef\]](#)
16. Russ PD, Allen-Davis JT, Weingardt JP, Anderson MS, Koyle MA. Mayer-Rokitansky-Küster-Hauser syndrome diagnosed by magnetic resonance imaging in a 15-year-old girl. *J Pediatr Adolesc Gynecol*. 1997;10(2):89-92. [\[CrossRef\]](#)
17. Strübbe E, Willemsen W, Lemmens J, Thijn C, Rolland RJA. Mayer-Rokitansky-Küster-Hauser syndrome: distinction between two forms based on excretory urographic, sonographic, and laparoscopic findings. *AJR Am J Roentgenol*. 1993;160(2):331-334.



# Susceptibility-Weighted Imaging Features of Meningiomas with Histopathologic Correlation

Onur Taydaş<sup>1</sup> , Ali Köksal<sup>2,3</sup> , Hayri Oğul<sup>4</sup> 

<sup>1</sup>Department of Radiology, Sakarya University, Faculty of Medicine, Sakarya, Turkey

<sup>2</sup>Department of Radiology, Bayindir Private Hospital, Ankara, Turkey

<sup>3</sup>Department of Radiology, Atılım University, Vocational School of Health Services, Ankara, Turkey

<sup>4</sup>Department of Radiology, Düzce University, Faculty of Medicine, Düzce, Turkey

**Cite this article as:** Taydaş O, Köksal A, Oğul H. Susceptibility-weighted imaging features of meningiomas with histopathologic correlation. *Current Research in MRI*. 2022; 1(2): 27-32.

**Corresponding author:** Hayri Oğul, e-mail: drhogul@gmail.com

**Received:** July 20, 2022 **Accepted:** August 19, 2022

**DOI:** 10.5152/CurrResMRI.2022.221526



Content of this journal is licensed under a Creative Commons Attribution-NonCommercial 4.0 International License.

## Abstract

**Objective:** The aim of the study was to investigate the characteristics of meningiomas, which are quite common tumors, in susceptibility-weighted imaging sequence which is increasingly used in magnetic resonance imaging in daily practice.

**Methods:** This study included 40 patients with intracranial meningioma between 2011 and 2017. The patients comprised 22 females and 18 males with a mean age of 47.7 years (range, 28-81 years). Magnetic resonance imaging with susceptibility-weighted imaging sequence and computed tomography were performed on all patients. The susceptibility score was calculated for each patient via susceptibility-weighted imaging sequence. Accordingly, less than 1/4 of the mass signal loss 1, 1/4-2/4 signal loss 2, 2/4-3/4 signal loss 3, and 3/4-4/4 signal loss were evaluated as 4 points.

**Results:** According to the pathologic World Health Organization classification, 21 of the patients (52.5%) had grade 1 (15 transitional, 3 meningothelial, 1 angiomatous, 1 microcystic, 1 psammomatous), 14 (35%) had grade 2 (all atypical), and 5 (12.5%) had grade 3 (all anaplastic) meningioma. Ten patients (25%) had calcification within the tumor in computed tomography. The median susceptibility score of the patients was 1. When age, tumor size, susceptibility score, and peripheral edema were compared with pathological grades, age (<0.001) and peripheral edema (0.009) were found to be statistically different.

**Conclusions:** Although meningiomas have different susceptibility-weighted imaging characteristics, this sequence has the potential to be used routinely in meningioma evaluation in the near future.

**Keywords:** A08—nervous system, computed tomography, magnetic resonance imaging, meningioma, susceptibility weighted imaging

## INTRODUCTION

Meningiomas are accounting for 16%-20% of all intracranial tumors.<sup>1</sup> The incidence increases with age.<sup>2</sup> It is about 2 times more common in women.<sup>3</sup> Most of the patients who do not have symptoms and are diagnosed incidentally have a stable course.<sup>4</sup> As the tumor grade increases, the probability of tumor invasion and malignancy increases.<sup>5</sup> Although magnetic resonance imaging (MRI) is the useful imaging modality for the evaluation of meningioma, computed tomography (CT) is also widely used in the initial evaluation.<sup>6</sup> However, in the diagnosis and follow-up of meningioma, MRI is the examination that should be used in order to evaluate a tumor invasion and to make a differential diagnosis. The diagnosis and follow-up of meningiomas are performed with high accuracy thanks to advanced MRI techniques that have become more common in recent years.<sup>7</sup>

One of the advanced MRI applications is the susceptibility weighted imaging (SWI) examination.<sup>8</sup> Although the major indications of the SWI sequence were neurovascular and neurodegenerative diseases, they are used successfully in many different diseases.<sup>9</sup> The aim of current study was to evaluate the characteristic findings of meningiomas, which are quite common tumors, in SWI sequence which is increasingly used in daily MRI practice. We also evaluated the association between histopathologic subtype and susceptibility score.

## METHODS

Magnetic resonance images of 40 patients with intracranial meningioma diagnosed between 2011 and 2017 were reviewed retrospectively. Spinal meningiomas were excluded from this study. Of our patients, 18 (45%) were male and 22 (55%) were female. The mean age of the patients was 47.7 years (range, 28-81 years).

Approval for the study was granted by the local ethics committee (12.02.2019-38/16), and all procedures were applied in accordance with the Helsinki Declaration. Informed consent was waived because of the retrospective nature of the study.

All MRI examinations were performed on a 1.5-T Magnet (Symphony Tim, Siemens Medical Systems, Germany). Axial and sagittal T1-weighted, axial fluid-attenuated inversion recovery (FLAIR), and axial T2-weighted images were taken. Susceptibility-weighted imaging sequence was

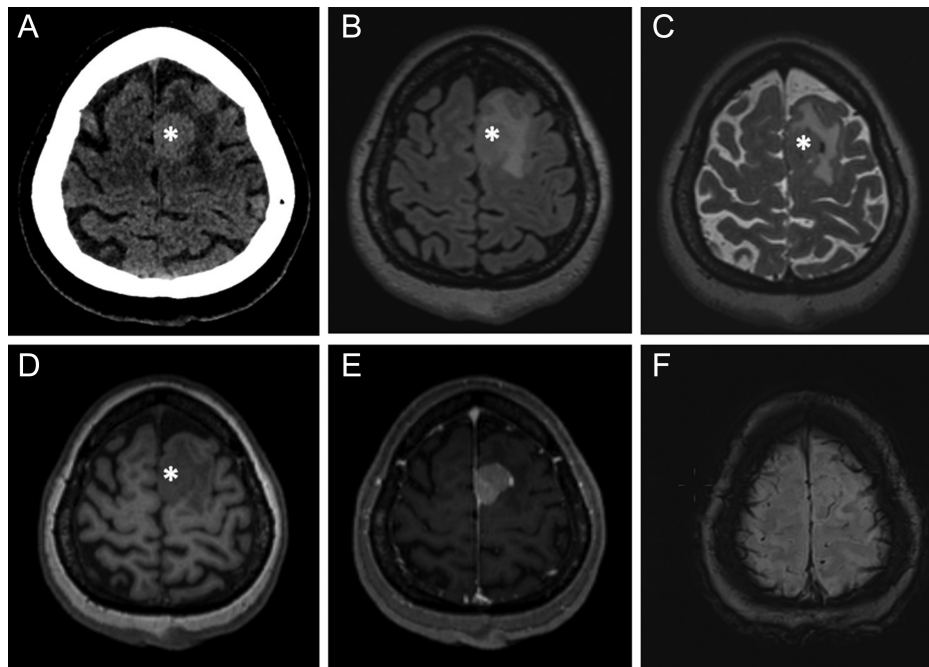


**Figure 1.** A 46-year-old woman was diagnosed with histopathologically WHO grade 3 anaplastic meningioma. Non-contrast axial CT scan (A) shows a parasagittal falx in meningioma (asterisk) in the left frontal. Axial FLAIR (B), T2 (C), and T1 (D) weighted MRI sequences show left frontal meningioma (asterisk) and its peripheral vasogenic edema. Post-contrast T1 (E) weighted MRI shows intense enhancement. In SWI sequence (F), the susceptibility score of the lesion is compatible with 0.

CT, computed tomography; FLAIR, fluid-attenuated inversion recovery; MRI, magnetic resonance imaging; SWI, susceptibility-weighted imaging; WHO, World Health Organization.

obtained in all the patients. The susceptibility score was calculated for each patient from the SWI sequence. Accordingly, less than 1/4 of the mass signal loss 1, 1/4-2/4 signal loss 2, 2/4-3/4 signal loss 3, and 3/4-4/4 signal loss were evaluated as 4 points. All of the patients were examined by CT (Emotion 16, Siemens Medical Systems, Germany) and the presence of calcification on CT images was evaluated. The images were retrospectively reviewed by two experienced radiologists. There was an agreement between them for each case. Pathological records were evaluated retrospectively to determine pathologic grade and tumor subtype.

For statistical analysis, MedCalc (Medcalc ver.12, Ostend, Belgium) was used. The chi-square test was performed for the comparison of categorical variables. The independent samples *t*-test was made for the comparison of continuous variables with normal distribution in the Kolmogorov–Smirnov and Shapiro–Wilk tests. Mann–Whitney *U* and Kruskal–Wallis tests were used to compare the data that did not conform to normal distribution according to the normality evaluation with

the Kolmogorov–Smirnov and Shapiro–Wilk tests. A value of  $P < .05$  was accepted as statistically significant.

## RESULTS

According to the pathologic World Health Organization (WHO) classification, 21 of the patients (52.5%) had grade 1 (15 transitional, 3 meningothelial, 1 angiomatous, 1 microcystic, and 1 psammomatous), 14 (35%) had grade 2 (all atypical), and 5 (12.5%) had grade 3 (all anaplastic) meningioma. Ten patients (25%) had calcification within the tumor in CT. Five patients had punctate, 4 had millimetric, and 1 had intense calcifications. The size of the lesions was  $42 \pm 20$  mm. In 15 patients (37.5%), the tumor was frontal, in 6 patients (15%) it was parietal, in 5 patients (12.5%), it was temporal, in 4 patients (10%), it was occipital, in 3 patients (7.5%), it was sphenoid wings, in 3 patients (7.5%), it was sphenoid wings, 2 patients (5%) had medullopontine angle, 1 patient (2.5%) had olfactory sulcus, and 1 patient (2.5%) had ethmoid roof tumor. Twenty-four patients (60%) had peripheral edema accompanying the tumor.

The susceptibility score was found to be 0 in 9 (22.5%) patients (Figure 1A-F), 1 in 17 patients (42.5%) (Figure 2A-D), 2 in 10 patients (25%) (Figure 3A-H), 3 in 3 patients (7.5%) (Figure 4A-F), and 4 in 1 patient (2.5%). When age, tumor size, susceptibility score, and peripheral edema were compared with pathological grades, age (Figure 5) and peripheral edema (Figure 6) were found to be statistically significant, respectively, with  $P < .001$  and  $P = .009$  (Table 1). When histological subtypes of grade 1 meningiomas were examined, no significant difference was found between the transitional subtype and other subtypes in terms of susceptibility score ( $P = .262$ ). There was no statistically significant difference in the susceptibility scores between the lesions with calcification on the CT and the lesions without calcification ( $P = .463$ ).

## MAIN POINTS

- Susceptibility-weighted imaging sequence can be used successfully in detecting calcifications in meningiomas.
- Susceptibility-weighted imaging of the advanced magnetic resonance imaging (MRI) applications has the potential to be used routinely in meningioma evaluation in the near future.
- On susceptibility-weighted imaging, meningiomas have different imaging characteristics.

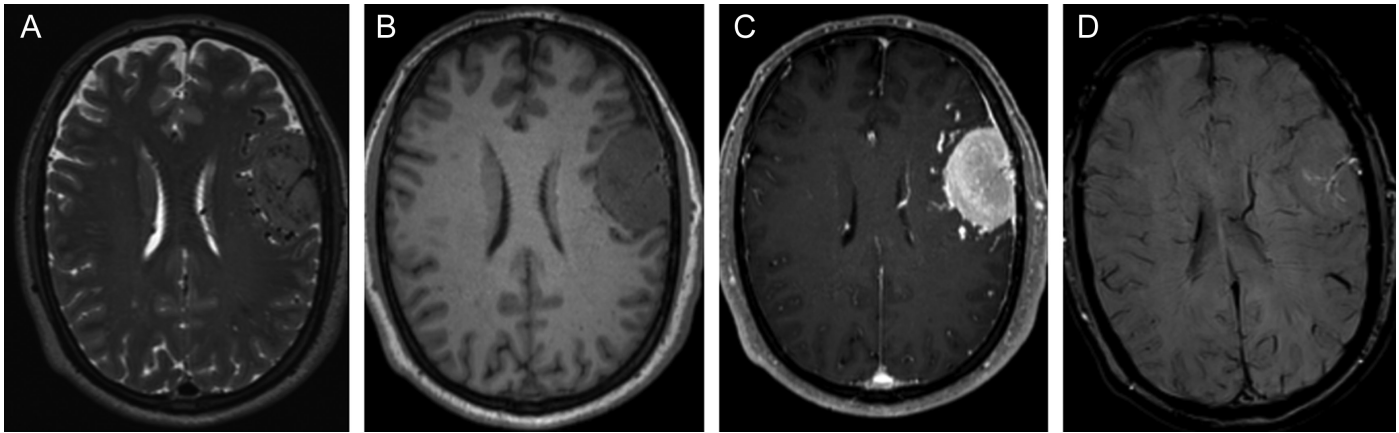


**Figure 2.** A 54-year-old man was diagnosed with histopathologically WHO grade 1 transitional meningioma. T2 (A) and T1 (B) weighted axial MRI show left frontal meningioma. Post-contrast T1 (C) weighted MRI shows intense enhancement. In SWI sequence (D), the susceptibility score of the lesion is compatible with 1. MRI, magnetic resonance imaging; SWI, susceptibility-weighted imaging; WHO, World Health Organization.

### DISCUSSION

Two previous studies have shown SWI sequence to be a reliable diagnostic tool in detecting magnetic susceptibility in meningiomas compared with routine MRI pulse sequences.<sup>10,11</sup> However, in these studies all patients had no correlation of SWI sequence with histopathologic findings. In a study by Schwyzer et al.<sup>10</sup> which included 36 patients, the

susceptibility and diffusion characteristics of meningiomas were compared. In this study, 36% of meningiomas were evaluated as SWI positive and ADC values were higher in SWI positive group. In our study, the median susceptibility score was 1 in the grade 1 group and 2 in the grade 2 and 3 groups. In the study by Adams et al.<sup>11</sup> CT and SWI were compared in the detection of calcifications in meningioma. In this study,

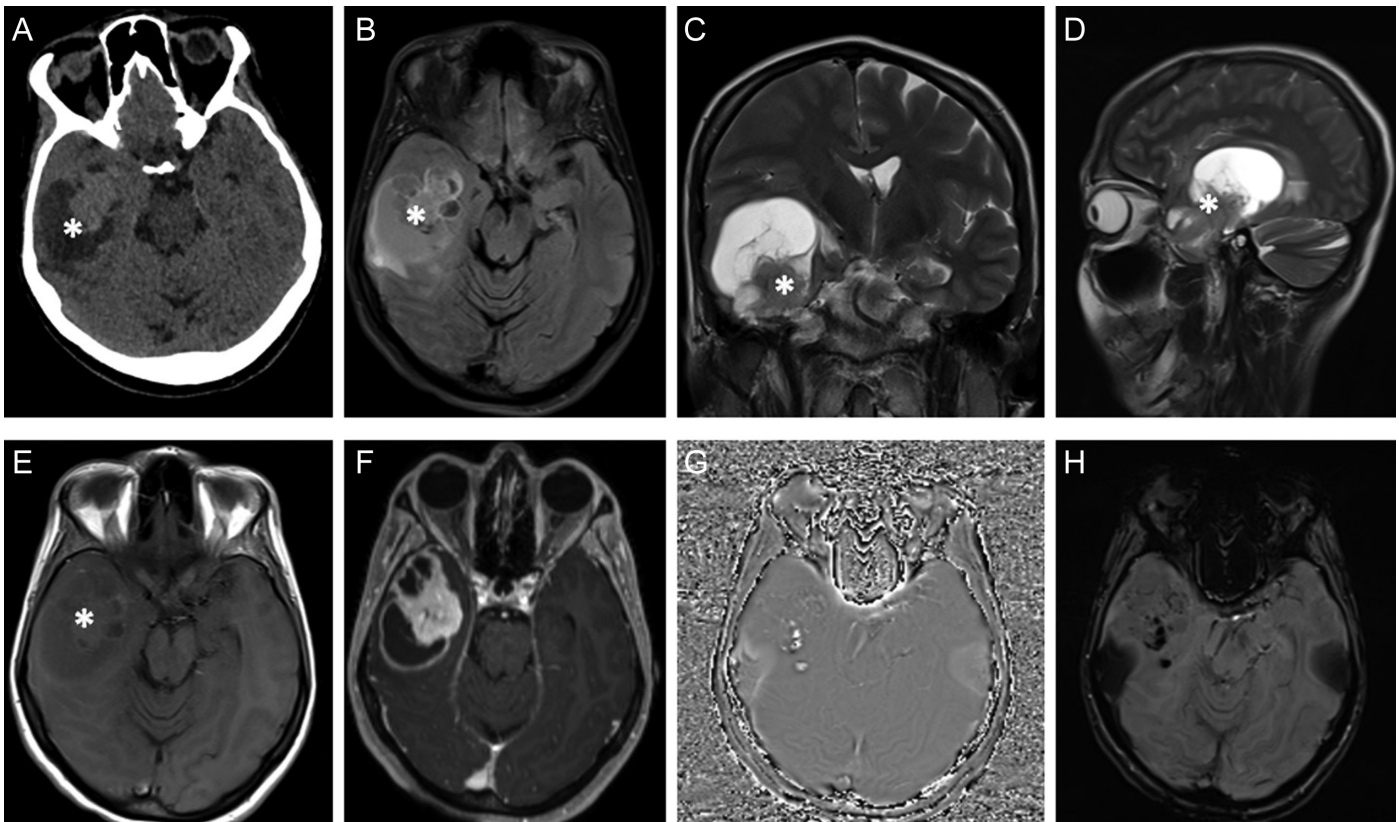


**Figure 3.** A 39-year-old woman was diagnosed with histopathologically WHO grade 3 anaplastic meningioma. Non-contrast axial CT scan (A) shows an extra-axial hypodense mass (asterisk) in the right temporal. Axial FLAIR (B), coronal T2 (C), sagittal T2 (D), and axial T1 (E) weighted MRI sequences show right middle cranial fossa meningioma (asterisk) and its peripheral vasogenic edema. Post-contrast T1 (F) weighted MRI shows intense enhancement in the solid component of the semisolid lesion. In phase image (G) and SWI (H) sequences, the susceptibility score of the lesion is compatible with 2. CT, computed tomography; FLAIR, fluid-attenuated inversion recovery; MRI, magnetic resonance imaging; SWI, susceptibility-weighted imaging; WHO, World Health Organization.



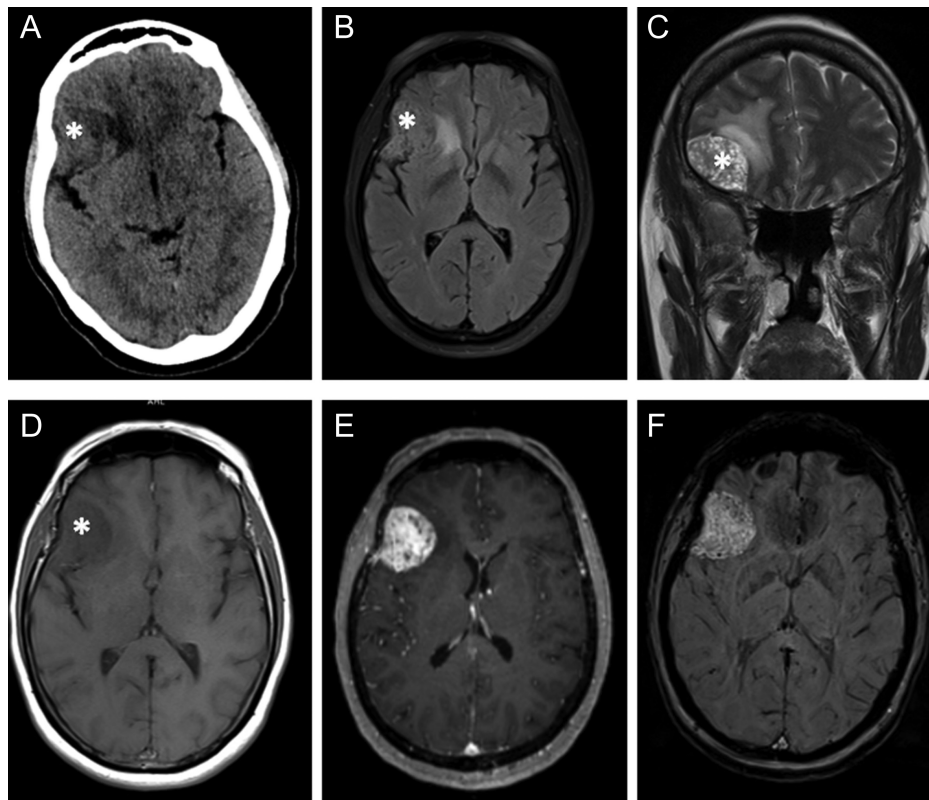


**Figure 4.** A 63-year-old woman was diagnosed with histopathologically WHO grade 1 meningioma. Non-contrast axial CT scan (A) shows an extra-axial mass (asterisk) in right orbitofrontal. Axial FLAIR(B), coronal T2 (C), and axial T1 (D) weighted MRI sequences show right anterior cranial fossa meningioma (asterisk) and its peripheral vasogenic edema. Post-contrast T1 (E) weighted MRI shows intense enhancement of the lesion. In SWI sequence (F), the susceptibility score of the lesion is compatible with 3. CT, computed tomography; FLAIR, fluid-attenuated inversion recovery; MRI, magnetic resonance imaging; SWI, susceptibility weighted imaging; WHO, World Health Organization.

SWI has been shown to be as successful as CT in detecting calcifications in meningiomas. In our study, 25% of the patients had calcification on the CT and all of these patients had calcification on the SWI examination.

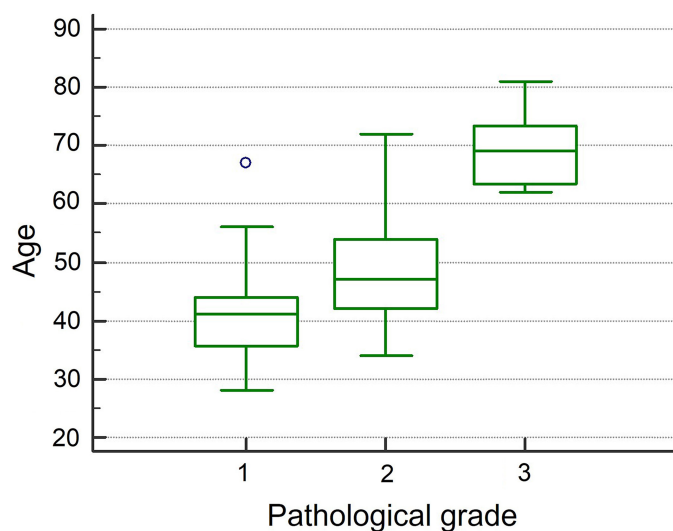


**Figure 5.** The graphic shows the correlation between age and pathological grade.

Meningiomas occur in the regions where the arachnoidal cells are intensively located. Many endogenous and exogenous factors may predispose to meningiomas. The most common exogenous factor is the ionizing radiation applied to the scalp region. Meningiomas are thought to have a role in the etiology of sex hormones because they are seen more frequently in women, they accelerate their growth during the luteal phase of pregnancy and menstrual cycle, and contain hormone receptors.<sup>12</sup> In the current study, the number of our patients of

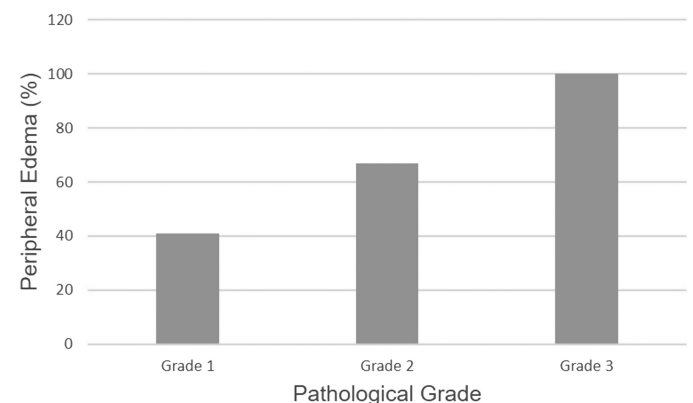


**Figure 6.** The graphic shows the correlation between peripheral edema and pathological grade.

**Table 1.** Comparison of Age, Tumor Size, Susceptibility Score, and Peripheral Edema According to Pathological Grade

	Grade 1	Grade 2	Grade 3	P
Age (mean)	41.6	49	69.4	<.001
Tumor size (mm, mean)	37.3	44.6	54.6	.410
Susceptibility score (median)	1	2	2	.285
Peripheral edema (percentage)	41%	67%	100%	.009

the female gender was higher. Meningiomas are usually dura-related, slow-growing benign tumors. They usually form masses of extra-axial growth, which are more repellent than neural parenchymal infiltration. Most meningiomas are located in intracranial, orbital, and intravertebral cavities. Meningioma development has been reported in almost all other organs, albeit quite rare. The most common location in the intracranial cavity is cerebral convexities, falx, and parasagittal area.<sup>13</sup> In our study, tumors were mostly located in the frontal, parietal, and temporal regions. Nine types of grade 1 (fibroblastic, meningothelial, transitional, angiomatous, psammomatous, secretory, microcystic, metaplastic, and lymphoplasma-rich), three grade 2 (clear-cell, chordoid, and atypical) and three grade 3 (rhabdoid, papillary, and anaplastic) meningioma subtypes have been defined in 2016 WHO classification of meningiomas of histopathological appearance. The recurrence rate was 7%-20% in grade 1 meningiomas, 30%-40% in grade 2 meningiomas, and 50%-80% in grade 3 meningiomas.<sup>5</sup> In our study, 21 of the patients (52.5%) had grade 1 (15 transitional, 3 meningothelial, 1 angiomatous, 1 microcystic, and 1 psammomatous), 14 (35%) had grade 2 (all atypical), and 5 (12.5%) had grade 3 (all anaplastic) meningioma.

Meningiomas appear to be iso (~40%) or hyperdense (~60%) extra-axial masses in CT without contrast. Calcifications can be found in the tumor (~25%). Contrast-enhanced CT shows intense and homogeneous enhancement. The formation of hyperostosis in neighboring bone (~20%) is an important feature.<sup>7</sup> Magnetic resonance imaging shows the whole extension of meningioma, vascular invasion, tumor vascularity, parenchymal edema, and intraosseous invasion, much better and more detailed than CT. In T1-weighted images, meningioma is mild hypointense similar to cerebral cortex, and T2-weighted images are mild hyperintense compared to gray matter. It shows intense enhancement after contrast agent.<sup>14,15</sup> The cleft sign defined for differentiation of extra-axial intradural lesions such as meningioma can be said between the lesion and brain tissue in the presence of cerebro spinal fluid (CSF), vascular, or hypointense dura. Dural tail is the name given to dural thickening extending from the sides of the lesion to the periphery and it is seen in 72% of meningiomas.<sup>16</sup>

Brain edema is not uncommon in meningiomas despite extra-axial localization.<sup>17</sup> Brain edema was found to be vasogenic in electron microscopy and diffusion-weighted images.<sup>18</sup> This finding suggests that the source of edema is caused by meningioma tissue rather than brain tissue. Vascular endothelial growth factor is thought to play an important role in edema formation. Vascular endothelial growth factor-induced pial vascularity and tumor vascularity are thought to be associated with peritumoral brain edema.<sup>19</sup> As a result of proliferation and prolongation of the meningioma through the arachnoid membrane, the brain barrier is impaired.<sup>20</sup> In the current study, the possibility of peripheral edema increased as the grade increased ( $P=.009$ ), although there was no statistically significant relationship between peripheral edema and tumor size ( $P=.258$ ). There are many publications in the literature showing that there is a relationship between grade and peripheral edema.<sup>21-23</sup> The relationship between tumor size and edema

is controversial. In some studies, no significant relationship was found between the size of the tumor and the amount of peritumoral edema.<sup>21,24</sup> However, there are also studies suggesting that large-sized tumors can lead to greater brain compressions, resulting in a reduction in venous return and associated ischemia and secondary peritumoral payment.<sup>25,26</sup>

There were several limitations of this study. First, the nature of the study was retrospective. Second, because of the retrospective nature of the study, sequence parameters could not be optimized. Finally, this study had a relatively small sample size.

In conclusion, although meningiomas have different SWI characteristics, this sequence has the potential to be used routinely in meningioma evaluation in the near future.

**Ethics Committee Approval:** Ethical committee approval was received from the Ethics Committee of Sakarya University (Date: February 12, 2019, Decision No: 38/16).

**Informed Consent:** Written informed consent was obtained from all participants who participated in this study.

**Peer-review:** Externally peer-reviewed.

**Author Contributions:** Concept – H.O.; Design – O.T.; Supervision – H.O.; Resources – H.O.; Materials – H.O.; Data Collection and/or Processing – H.O.; O.T.; Analysis and/or Interpretation – H.O.; Literature Search – H.O., A.K.; Writing Manuscript – H.O., O.T.; Critical Review – H.O.; Other – A.K.

**Declaration of Interests:** The authors have no conflicts of interest to declare.

**Funding:** The authors declared that this study has received no financial support.

## REFERENCES

- Toh CH, Castillo M, Wong AM, et al. Differentiation between classic and atypical meningiomas with use of diffusion tensor imaging. *AJNR Am J Neuroradiol*. 2008;29(9):1630-1635. [\[CrossRef\]](#)
- Netsky MG, Lapresle J. The first account of a meningioma. *Bull Hist Med*. 1956;30:465-468.
- Alexiou GA, Gogou P, Markoula S, Kyritsis AP. Management of meningiomas. *Clin Neurol Neurosurg*. 2010;112(3):177-182. [\[CrossRef\]](#)
- Bondy M, Ligon BL. Epidemiology and etiology of intracranial meningiomas: a review. *J Neurooncol*. 1996;29(3):197-205. [\[CrossRef\]](#)
- Louis DN, Perry A, Reifenberger G, et al. The 2016 World Health Organization classification of tumors of the central nervous system: a summary. *Acta Neuropathol*. 2016;131(6):803-820. [\[CrossRef\]](#)
- Saloner D, Uzelac A, Hetts S, Martin A, Dillon W. Modern meningioma imaging techniques. *J Neurooncol*. 2010;99(3):333-340. [\[CrossRef\]](#)
- Lyndon D, Lansley JA, Evanson J, Krishnan AS. Dural masses: meningiomas and their mimics. *Insights Imaging*. 2019;10(1):11. [\[CrossRef\]](#)
- Haacke EM, Mittal S, Wu Z, Neelavalli J, Cheng YC. Susceptibility-weighted imaging: technical aspects and clinical applications, part 1. *AJNR Am J Neuroradiol*. 2009;30(1):19-30. [\[CrossRef\]](#)
- Mittal S, Wu Z, Neelavalli J, Haacke EM. Susceptibility-weighted imaging: technical aspects and clinical applications, part 2. *AJNR Am J Neuroradiol*. 2009;30(2):232-252. [\[CrossRef\]](#)
- Schwyzler L, Berberat J, Remonda L, Roelcke U. Susceptibility changes in meningiomas influence the apparent diffusion coefficient in diffusion-weighted MRI. *J Neuroimaging*. 2015;42(6):332-337. [\[CrossRef\]](#)
- Adams LC, Böker SM, Bender YY, et al. Assessment of intracranial meningioma-associated calcifications using susceptibility-weighted MRI. *J Magn Reson Imaging*. 2017;46(4):1177-1186. [\[CrossRef\]](#)
- Buerki RA, Horbinski CM, Kruser T, Horowitz PM, James CD, Lukas RV. An overview of meningiomas. *Future Oncol*. 2018;14(21):2161-2177. [\[CrossRef\]](#)
- Backer-Grøndahl T, Moen BH, Torp SH. The histopathological spectrum of human meningiomas. *Int J Clin Exp Pathol*. 2012;5(3):231-242.
- O'Leary S, Adams WM, Parrish RW, Mukonoweshuro W. Atypical imaging appearances of intracranial meningiomas. *Clin Radiol*. 2007;62(1):10-17. [\[CrossRef\]](#)

15. Watts J, Box G, Galvin A, Brochie P, Trost N, Sutherland T. Magnetic resonance imaging of meningiomas: a pictorial review. *Insights Imaging*. 2014;5(1):113-122. [\[CrossRef\]](#)
16. Huang RY, Bi WL, Griffith B, et al. Imaging and diagnostic advances for intracranial meningiomas. *Neuro Oncol*. 2019;21(Suppl 1):i44-i61. [\[CrossRef\]](#)
17. Bitzer M, Opitz H, Popp J, et al. Angiogenesis and brain oedema in intracranial meningiomas: influence of vascular endothelial growth factor. *Acta Neurochir (Wien)*. 1998;140(4):333-340. [\[CrossRef\]](#)
18. Bitzer M, Klose U, Geist-Barth B, et al. Alterations in diffusion and perfusion in the pathogenesis of peritumoral brain edema in meningiomas. *Eur Radiol*. 2002;12(8):2062-2076. [\[CrossRef\]](#)
19. Osawa T, Tosaka M, Nagaishi M, Yoshimoto Y. Factors affecting peritumoral brain edema in meningioma: special histological subtypes with prominently extensive edema. *J Neurooncol*. 2013;111(1):49-57. [\[CrossRef\]](#)
20. Schmid S, Aboul-Enein F, Pfisterer W, Birkner T, Stadek C, Knosp E. Vascular endothelial growth factor: the major factor for tumor neovascularization and edema formation in meningioma patients. *Neurosurgery*. 2010;67(6):1703-1708. [\[CrossRef\]](#)
21. Kim BW, Kim MS, Kim SW, Chang CH, Kim OL. Peritumoral brain edema in meningiomas: correlation of radiologic and pathologic features. *J Korean Neurosurg Soc*. 2011;49(1):26-30. [\[CrossRef\]](#)
22. Azizyan A, Eboli P, Drazin D, Mirocha J, Maya MM, Bannykh S. Differentiation of benign angiomatous and microcystic meningiomas with extensive peritumoral edema from high grade meningiomas with aid of diffusion weighted MRI. *BioMed Res Int*. 2014;2014:650939. [\[CrossRef\]](#)
23. Hsu CC, Pai CY, Kao HW, Hsueh CJ, Hsu WL, Lo CP. Do aggressive imaging features correlate with advanced histopathological grade in meningiomas? *J Clin Neurosci*. 2010;17(5):584-587. [\[CrossRef\]](#)
24. Gurkanlar D, Er U, Sanlı M, Özkan M, Sekerci Z. Peritumoral brain edema in intracranial meningiomas. *J Clin Neurosci*. 2005;12(7):750-753. [\[CrossRef\]](#)
25. Tamiya T, Ono Y, Matsumoto K, Ohmoto T. Peritumoral brain edema in intracranial meningiomas: effects of radiological and histological factors. *Neurosurgery*. 2001;49(5):1046-1051. [\[CrossRef\]](#)
26. Lee KJ, Joo WI, Rha HK, et al. Peritumoral brain edema in meningiomas: correlations between magnetic resonance imaging, angiography, and pathology. *Surg Neurol*. 2008;69(4):350-355. [\[CrossRef\]](#)



# Can We Predict Triple Negative Breast Cancer with Magnetic Resonance Imaging Findings?

Eda Cingöz<sup>1</sup> , Rana Günöz Cömert<sup>2</sup> , Zuhale Bayramoğlu<sup>1</sup> , Neslihan Cabioğlu<sup>3</sup> , Ravza Yılmaz<sup>1</sup> 

<sup>1</sup>Department of Radiology, İstanbul University, Faculty of Medicine, İstanbul, Turkey

<sup>2</sup>Department of Radiology, Turhal Hospital, Tokat, Turkey

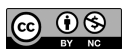
<sup>3</sup>Department of General Surgery, İstanbul University, Faculty of Medicine, İstanbul, Turkey

**Cite this article as:** Cingöz E, Günöz Cömert R, Bayramoğlu Z, Cabioğlu N, Yılmaz R. Can we predict triple-negative breast cancer with magnetic resonance imaging findings? *Current Research in MRI*. 2022; 1(2): 33-37.

**Corresponding author:** Eda Cingöz, e-mail: edacanipek@gmail.com

**Received:** September 1, 2022 **Accepted:** October 26, 2022

DOI:10.5152/CurrResMRI.2022.220307



Content of this journal is licensed under a Creative Commons Attribution-NonCommercial 4.0 International License.

## Abstract

**Objective:** Triple-negative breast cancer comprises a small percentage of all breast cancers. However, they are accountable for a high percentage of the loss of lives. Being able to predict triple-negative breast cancer by imaging may play a pivotal role in earlier management and the planning of the treatment. We scrutinized imaging features for 64 patients diagnosed with triple-negative breast cancer on magnetic resonance imaging to define the characteristic findings in imaging. An additional objective was to define the spectrum of imaging findings concerning triple-negative breast cancer in mammography as well as ultrasonography.

**Methods:** In this descriptive study, between 2018 and 2022, 64 patients diagnosed with triple-negative breast cancer and underwent magnetic resonance imaging were enrolled in our present study. Imaging findings were evaluated based on the (Breast Imaging Reporting and Data System) (BI-RADS) Atlas, fifth edition.

**Results:** Triple-negative breast cancer was more often localized posteriorly in 29 patients (45%). Fifty-five (86%) of the 64 lesions revealed mass enhancement. The internal enhancement patterns were mostly in the rim (36%) and heterogeneous pattern (42%). Masses were commonly round/oval-shaped (63.6%) with irregular margins (51%). It was seen unifocally in 40 (63%) of the patients. The early enhancement was average in 25 (39%) and rapid in 22 (34%) patients, with washout delay enhancement in 24 of 55 cases. Intratumoral copiously high signal occurred in 22 (34%) and high signal intensity in 20 (31%) on T2-weighted images. Round/oval-shaped masses with indistinct margins were common findings in mammography and ultrasonography.

**Conclusion:** Our results show that triple-negative breast cancer is typically seen as a round/oval-shaped mass with irregular margins and rim-heterogeneous enhancement. Also, triple-negative breast cancer is most commonly related to a very high T2 signal intensity, and they are usually found as unifocal lesions.

**Keywords:** Breast, carcinoma, magnetic resonance imaging

## INTRODUCTION

Breast cancer is one of the complicated morbidities with varied morphological, biological, and molecular characteristics.<sup>1</sup> Triple-negative breast cancer (TNBC) comprises approximately 10-20% of all breast cancers that do not express human epidermal growth factor receptor 2 (HER2), estrogen receptors (ER), or progesterone receptors (PR).<sup>2-4</sup> It is defined by different molecular, histological, and clinical findings inclusive of an especially negative prognosis. Triple-negative breast cancers and basal-like breast cancers are closely related but are not synonymous or interchangeable. Basal-like cancers are frequently related to the high histologic grade, mutation of the TP53 gene, suppressed BRCA1 function, and a bad prognostic result. These are known as aggressive features.<sup>5</sup> Magnetic resonance imaging (MRI) is the most sensitive imaging technique for the diagnosis of breast cancer and that is why it is specified prior to operation to show the scope of the disease. Magnetic resonance imaging can provide significant data not only on the shape of the masses but also on the pathology represented by the signal intensity features and on the dynamic evaluation of contrast medium uptake. Had it been possible to predict TNBC based on MRI features, these findings would provide both pretreatment planning and prognostic information. There have been a few studies on the relationship between TNBC and MRI features.<sup>6-8</sup> The goal of our work was to define the MRI features of TNBC and to reveal whether the diagnostic abilities of MRI could be used to credibly estimate the status of TNBC prior to tissue biopsy results becoming obtainable. An additional aim was to describe the characteristics of imaging features regarding triple-negative cancers on both mammography (MG) and ultrasonography (US).

## METHODS

### Patients

All TNBCs between May 2012 and December 2016 were reviewed, and 64 (56 invasive ductal carcinomas, 7 metaplastic carcinomas, and 1 invasive lobular carcinoma) patients who received MRI in our institution were taken into this study after informed consents were provided from all of the participants. Immunohistochemical analysis of ER, PR, and HER2 status had been performed on breast tissue materials attained from surgery and ER and PR's status was considered to be negative if the expression was less than 10%. The histopathological preparations were tested

for HER2 gene expression using a validated dual-probe fluorescence in situ hybridization. Triple-negative breast cancers are defined by the lack of the 3 predictive/prognostic markers: ER, PR, and HER2. The study was approved by the ethics committee of Istanbul University (Date: July 29, 2022, Decision no: 2022/1296).

### Ultrasonography and Mammography

Two radiologists experienced in breast imaging (1 with 7 years and the other with 4 years of experience) evaluated all images and evaluated the images according to the BI-RADS (Breast Imaging Reporting and Data System) Atlas, fifth edition Radiology.<sup>9</sup> Ultrasonography (Acuson Antares; Siemens, Germany) was performed on all patients via a high-resolution linear probe with a 12 MHz frequency. Women underwent MG by bilateral 2-view full-field digital MG (Giotto; Bologna, Italy).

### Magnetic Resonance Imaging

Studies were exerted at 1.5-T on an MRI unit (Achieva; Philips Medical Systems, Best, The Netherlands). A dedicated 4-channel phased-array breast coil was used in the prone position. Each MRI examination included a T1-weighted (T1-W) sequence (TR [Time of Repetition]/TE [Time of Excitation]: 495/8 ms; FOV (Field of View), 340 × 400 mm; NEX (Number of Excitation), 2; slice thickness, 2 mm; matrix, 272 × 267) in the axial plane and fat-saturated T2-weighted (T2-W) images in the axial plane using turbo spin-echo sequence (TR/TE: 4130/118 ms; FOV, 340 × 340 mm; NEX, 3; slice thickness, 2 mm; matrix, 272 × 224) were performed. In the T1-W turbo field-echo 3-dimensional sequences (TR/TE, 6.8/3.3 ms; NEX, 3; FOV, 340 × 340 mm; matrix, 340 × 338), dynamic images were taken once before and 5 times following the injection of the contrast agent including 0.1 mmol/kg gadolinium. Lesions of the time-signal intensity curves were plotted and commented. In patients with multifocal tumors, we assessed only the index mass in order to perform a statistical analysis of the correlation between the histological and the MRI findings. Lesions were divided into 3 categories: focus, mass, and non-mass enhancement. Masses were scrutinized with regard to shape (irregular, round, or oval), margin (smooth, spiculated, or irregular), and characteristic features of internal enhancement pattern (heterogeneous, homogeneous, or rim enhancement). Non-mass enhancement was described in terms of distribution (focal, linear, segmental, regional/multiple regional, or diffuse) and internal enhancement (heterogeneous, homogeneous, clumped, or clustered ring). The initial contrast uptake and late contrast enhancement-time intensity curve images were obtained by post-processing with MRI software. We evaluated MRI kinetics in terms of the most suspicious kinetics pattern. Background parenchymal enhancement obtained with the second contrast-enhanced sequence is categorized as minimal, mild, moderate, or marked, and also either symmetric or asymmetric was described. The amount of fibroglandular

tissue, the long and short diameters of the tumor, the intensity of mass, and parenchyma edema on the T2-W image were documented. Skin retraction-thickening-invasion and nipple retraction-invasion and invasion to pectoral muscle, presence of cyst, and distortion were detected. The tumor locations were classified as quadrant locations and antero-posterior localization (1/3 anterior, 1/3 middle, 1/3 posterior, and extensive). The type of the disease was categorized as 1 of 3 types. The unifocal type was described when just 1 single malignant focus was encountered, the multifocal type was described when more than 1 malignant focus was encountered in the same quadrant, and the multicentric type was described when more than 1 malignant focus was revealed in more than 1 quadrant. In multifocal and multicentric cases, in addition to the index lesion, at least 1 biopsy was performed from a malignant focus. The biopsy results were exactly compatible with the analyzed lesion on MRI. The study was conducted in a descriptive fashion. Mean ± standard deviation and median with range data are presented. The frequencies of the findings of magnetic resonance studies were also evaluated.

### RESULTS

Mammography and US features of an index tumor were documented in multifocal and multicentric patients. Our study population's MG findings are shown in Table 1. Eight mammograms were normal in TNBC. The most common mammographic finding was mass appearance in 53 (82.7%) patients. Masses without calcification were most common on 41 (64%) mammograms. Ultrasonography revealed masses in all patients, including the 8 cancers determined to be occult on MG. Ultrasonography findings are documented in Table 2. Triple-negative breast cancer mostly showed masses with round/oval shape in 37 cases (57.8%) and indistinct margins in 40 (62.5%). Fifty-one of the TNBCs (79.6%) were hypoechoic and 34 of them (53.1%) had no posterior acoustic features. The mean age was 47.5 years (range 28-72). The mean size of the tumors was short diameter 2.6 cm (range 0.3-10 cm) and long diameter 3.6 cm (range 0.4-11 cm) (Table 3). Superior-outer quadrant represented the most common localization in 40 patients (63%). The amount of fibroglandular tissue was type A in 2 (3%), type B in 15 (23%), type C in 28 (44%), and type D in 19 (30%). Background parenchymal enhancement was minimal in 17 (26%), mild in 28 (44%), moderate in 12 (19%), and marked in 7 (11%). Triple-negative breast cancers were located 1/3 posterior in 29 patients (45%), middle 1/3 segment in 17 (26%), 1/3 anterior in 8 (13%), and both 1/3 posterior and 1/3 middle segment that was classified as extensive in 10 of them (16%). As a result, TNBCs were located posteriorly in 39 of 55 patients (61%). Very high signal intensity was seen in 22 (34%), high signal intensity in 20 (31%), and hypointense/isointense was seen in 22 (34%) patients on T2-W images. Parenchyma edema was

### MAIN POINTS

- While triple-negative breast cancer constitutes a small percentage of all breast cancers, it has an enormous contribution to deaths from breast cancer.
- Certain magnetic resonance imaging findings including round/oval-shape, rim or heterogeneous enhancement, high signal intensity on T2-weighted images, and posterior-prepectoral location could direct the diagnosis to triple-negative breast cancer.
- Triple-negative breast cancer tends to be seen in more dense and heterogeneous breasts.

**Table 1.** Mammographic Features in Triple-Negative Breast Cancer

		Frequency (Percent)
Mammographic findings	Normal	12
	Mass only	64
	Mass with calcification	19
	Calcification	2
	Focal asymmetry	3
Mass shape	Round/oval	55
	Irregular	45
Mass margin	Circumscribed	17
	Microlobulated	13
	Obscured	15
	Indistinct	55

**Table 2.** Ultrasound Features of Triple-Negative Breast Cancer

		Frequency (Percent)
Mass shape	Round/oval	58
	Irregular	42
Mass margin	Circumscribed	9
	Indistinct	63
	Angular	12
	Microlobulated	16
Echo pattern	Hypoechoic	80
	Complex	12
	Isoechoic	8
Posterior acoustic features	None	53
	Enhancement	31
	Shadowing	6
	Combined	10

minimal in 12 (19%) and prominent in 32 (50%) patients. Fifty-five (86%) of the 64 TNBCs revealed as a mass, and the other 9 (14%) had non-mass enhancement. None of the triple-negative cancers was evaluated as a focus. The 55 TNBCs with mass appearance were frequently round/oval-shaped (64%) and irregular-shaped (36%). Mass margins were irregular in 28 (51%), spiculated in 10 (18%), and smooth in 17 (31%) of the masses. The predominant pattern of internal enhancement of mass was founded as rim enhancement which was seen in 20 (36%) of the 55 patients. Heterogeneous enhancement was monitored in 23 of the 55 cases (42%) and homogeneous enhancement was monitored in 12 of them (22%). All metaplastic cancers appeared as masses with rim enhancement. Only 1 case of invasive lobular cancer showed

**Table 3.** Magnetic Resonance Imaging Features of Triple-Negative Breast Cancer

		Frequency (Percent)
Location	Anterior	8
	Middle	17
	Posterior	29
T2 sequence signal	Hypoiso-intense	22
	Hyperintense	20
	Very hyperintense	22
Mass/non-mass	Mass	55
	Non-mass	9
Mass shape	Round/oval	64
	Irregular	36
Mass margin	Smooth	31
	Spiculated	18
	Irregular	51
Mass enhancement	Heterogeneous	23
	Rim	20
	Homogeneous	22
Non-mass enhancement	Heterogeneous	56
	Clumped	28
Non-mass distribution	Diffuse	33
	Regional	11
	Segmental	55
Early enhancement	Slow	27
	Medium	39
	Fast	34
Delay enhancement	Persistent	26
	Plateau	36
	Washout	38

non-mass enhancement with an internal heterogeneous enhancement of diffuse distribution. Magnetic resonance imaging showed 4 only one mass in 40 (63%) of the patients, multifocality in 13 (20%), and multicentricity in 11 (17%). The most common pattern regarding internal enhancement was heterogeneous (56%) in the 9 patients with non-mass enhancement. Three of them reviewed diffuse distribution, 5 of them showed segmental distribution, and only 1 cancer showed multiple regional enhancements. Focus, focal, and linear enhancement patterns were not seen. The early enhancement patterns were mostly medium in 25 (39%) and fast in 22 (34%) of our patients. The delay enhancement patterns were washout, as observed in 24 (38%), and plateau in 23 (36%). A persistent time-intensity pattern was noted in 17 cases (Table 3). Skin changes were seen in 20 patients. Skin retraction-thickening-invasion were seen in 15, 2, and 3 patients, respectively. No cyst was seen in 48 patients. Distortion accompanying mass was seen in 21 patients (33%). Seven patients had nipple retraction and 3 of them had nipple involvement, and 5 patients had invasion to pectoral muscle and this finding was visualized only on MRI. Necrosis was seen in 26 (41%) patients. Mean value of Ki-67 was 71 with a range of 5-95. Ki67 was positive in 89% of cases (57 of 64), with a cutoff value of 50%.

## DISCUSSION

Triple-negative breast cancers have no targeted treatment that has been performed effectively. However, they are responsible for a comparatively excessive number of deaths related to breast cancer, often due to aggressive clinical courses.<sup>10</sup> Thus, advanced knowledge of this molecular subtype of breast cancer is required for the proper management of patients. Imaging features are of paramount importance because the more we know about the imaging characteristics of molecular subtypes, the better we can predict the course of the disease. On MG and US, TNBC can mimic lesions with benign morphology.<sup>11-13</sup> Triple-negative breast cancer has been found to be an oval/round mass that is very rarely accompanied by calcification on MG similar to our findings.<sup>7,14</sup> On US, they were likely to be hypoechoic or markedly hypoechoic masses with an irregular or oval/round shape and mostly circumscribed margins in the literature.<sup>15</sup> Against the circumscribed margin of these studies on MG and US, our results suggest TNBCs were mostly oval/round masses but with indistinct margins.<sup>7,14,15</sup> Due to dense breast or benign or unclear MG and ultrasound features, TNBC can be more difficult to diagnose by MG or US.<sup>11-13,16,17</sup> In addition to TNBC, Schrading and Kuhl<sup>18</sup> declared that familial breast cancers tend to occur with benign morphologic features. Magnetic resonance imaging is quite successful in this type of cancer diagnosis compared with conventional methods because of more evident malign findings.<sup>15</sup> Our results show that TNBCs are more frequently mass lesions, round or oval-shaped, irregular margin, and rim or heterogeneous enhancement (Figure 1). Also, MRI findings of TNBC were high signal intensity on T2-W images (65%) and a unifocal lesion (63%) (Figure 2). These features were consistent with typical TNBC features previously reported.<sup>6,7,11,14,15</sup> Uematsu et al<sup>6</sup> have reported that a significantly high signal in tumors on T2-W was related to TNBC and also considerably related to necrosis. Twenty-nine (41%) of the TNBC showed necrosis in our study. Respecting enhancement kinetics, features of different delay enhancement patterns have been reported,<sup>6,7</sup> and in our study, 74% of TNBC showed a washout and plateau enhancement pattern. The early enhancement patterns were medium and fast in 73% of our patients, which makes facilitating differentiation between benign and malignant tumors difficult. Multifocal and multicentric disease is frequently encountered in luminal B and HER2 subtypes, compared with luminal A and TNBC.<sup>19,20</sup> Preoperative breast MRI may be very helpful in better defining the extent of disease for patients of luminal B and HER2



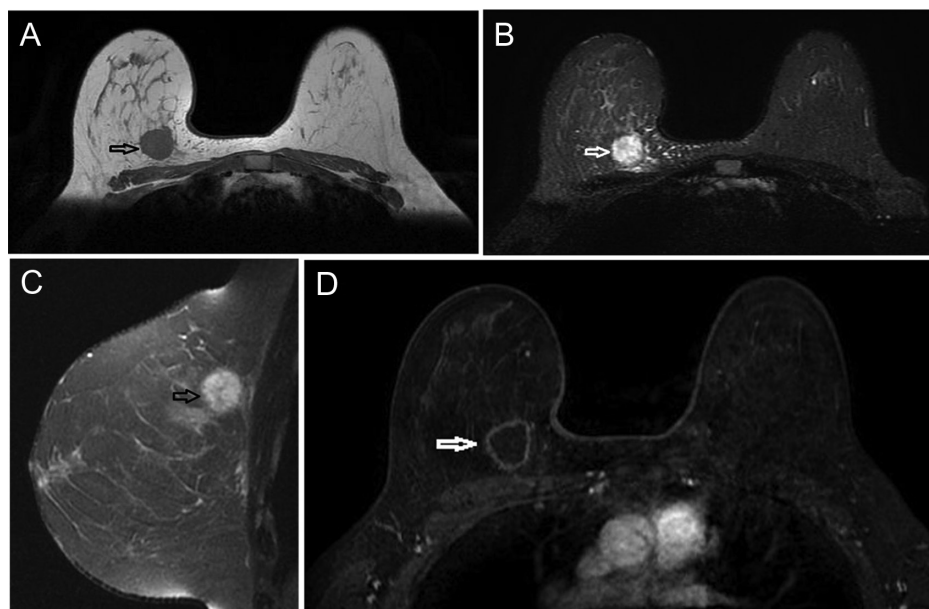


**Figure 1.** Triple-negative breast cancer is in a 45-year-old woman's right breast. T1-weighted (T1-W) (A) and T2- weighted (T2-W) with fat saturation (B) axial MR images show a 1.5-cm round mass with an irregular margin in the posterior location (black arrow in A and white arrow in B). Very high signal intensity mass and prominent peritumoral edema is seen in fat-saturated T2-W axial image. Hyperintense mass (C) is also seen adjacent to the pectoral muscle (black arrow) in the same sequence at sagittal view. The T1-W subtraction image (D) reveals the mass with rim enhancement (white arrow).

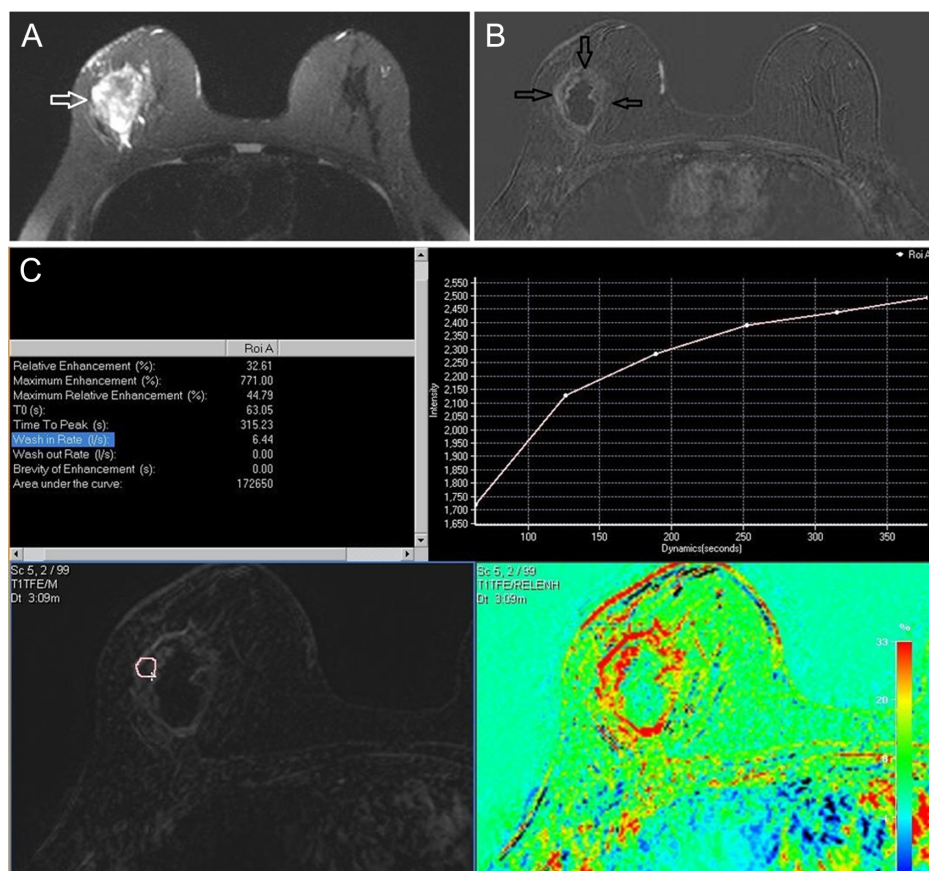


**Figure 2.** A 43-year-old woman with palpable triple-negative breast cancer of the right breast. T2-weighted with fat saturation image (A) demonstrates a 4.5-cm hyperintense mass with irregular margin and peritumoral edema in both middle and posterior segments (white arrow). Mass with irregular rim enhancement (black arrows) is seen on the postcontrast T1-weighted subtraction image (B). Measurements made from the periphery of the lesion showed a type 1 curve and areas in pink indicate a delayed persistent-type curve following slow early enhancement (C).

subtypes. Triple-negative breast cancer more commonly showed rim enhancement on postcontrast MRI and more high intratumoral signal intensity on T2-W than other tumor subtypes.<sup>15</sup> Besides morphological and kinetic analyses, location is useful for the diagnosis of TNBC. Our findings revealed that 67% of TNBC tend to locate in a posterior or prepectoral region. Breast cancers in familial high-risk women and BRCA1 mutation carriers were located in the posterior or prepectoral region of the breast without analyzing the results according to tumor subtype as observed by Schrading and Kuhl.<sup>18</sup> One study showed that TNBCs were commonly located in the posterior third or prepectoral region of the breast in accordance with our study.<sup>21</sup> Mammography and US may be insufficient to detect this type of breast cancer. It can be skipped in MG, especially when combined with dense parenchyma and may be difficult to visualize deep plans in breasts with a heterogeneous background with US. In order to detect this aggressive tumor, we need to evaluate this region of the breast carefully. Magnetic resonance imaging is superior to MG and US in evaluating the posterior part of the breast, particularly in dense and heterogeneous parenchyma. In our study, the amount of fibroglandular tissue was type C and D, with a total rate of 74% seen in patients with TNBC. One limitation of this study was that it was a retrospective design. We consider that in the future MRI will help in the characterization and treatment plan of the different subtypes of breast cancer and that more studies will be required.

## CONCLUSION

Magnetic resonance imaging findings such as round/oval-shaped, rim or heterogeneous enhancement, high signal intensity on T2-W images, and posterior-prepectoral location may be important in diagnosing TNBC. These findings may allow us to estimate the diagnosis of TNBC before the histopathological diagnosis. Moreover, because of common localization and to be seen in more dense and heterogeneous breasts, TNBC can be diagnosed more easily with MRI.

**Ethics Committee Approval:** The study was approved by the ethics committee of Istanbul University (Date: July 29, 2022, Decision no: 2022/1296).

**Informed Consent:** Written informed consent was obtained from all participants who participated in this study.

**Peer-review:** Externally peer-reviewed.

**Author Contributions:** Concept – R.Y., N.C.; Design- R.Y., Z.B.; Supervision- R.Y., N.C.; Materials- E.C., R.G.C.; Data collection and processing- R.Y., Z.B., E.C., R.G.C.; Analysis and interpretation- R.Y., Z.B.; Literature Review- Z.B., E.C., R.G.C.; Writing- Z.B., E.C., R.G.C.; Critical Review- R.Y.

**Declaration of Interests:** The authors have no conflicts of interest to declare.

**Funding:** The authors declared that this study has received no financial support.

## REFERENCES

- Yanagawa M, Ikemoto K, Kawauchi S, et al. Luminal A and luminal B (HER2 negative) subtypes of breast cancer consist of a mixture of tumors with different genotype. *BMC Res Notes*. 2012;5:376. [\[CrossRef\]](#)
- Yao H, He G, Yan S, et al. Triple-negative breast cancer: is there a treatment on the horizon? *Oncotarget*. 2017;8(1):1913-1924. [\[CrossRef\]](#)
- Newman LA, Reis-Filho JS, Morrow M, Carey LA, King TA. The 2014 Society of Surgical Oncology Susan G. Komen for the Cure Symposium: triple-negative breast cancer. *Ann Surg Oncol*. 2015;22(3):874-882. [\[CrossRef\]](#)
- Damaskos C, Garmpi A, Nikolettos K, et al. Triple-negative breast cancer: the progress of targeted therapies and future tendencies. *Anticancer Res*. 2019;39(10):5285-5296. [\[CrossRef\]](#)
- Silwal-Pandit L, Vollan HK, Chin SF, et al. TP53 mutation spectrum in breast cancer is subtype specific and has distinct prognostic relevance. *Clin Cancer Res*. 2014;20(13):3569-3580. [\[CrossRef\]](#)
- Uematsu T, Kasami M, Yuen S. Triple-negative breast cancer: correlation between MR imaging and pathological findings. *Radiology*. 2009;250(3):638-647. [\[CrossRef\]](#)
- Dogan BE, Gonzalez-Angulo AM, Gilcrease M, Dryden MJ, Yang WT. Multimodality 1 imaging of triple receptor-negative tumors with mammography, ultrasound, and MRI. *AJR Am J Roentgenol*. 2010;194(4):1160-1166. [\[CrossRef\]](#)
- Uematsu T. MR imaging of triple-negative breast cancer. *Breast Cancer*. 2011;18(3):161-164. [\[CrossRef\]](#)
- Sickles EA, D'Orsi C. Follow-up and outcome monitoring. In: *ACR BIRADS® atlas, breast imaging and reporting and data system*. Reston, VA: American College of Radiology; 2013:27.
- Jitariu AA, Cimpean AM, Ribatti D, Raica M. Triple negative breast cancer: the kiss of death. *Oncotarget*. 2017;8(28):46652-46662. [\[CrossRef\]](#)
- Du HY, Lin BR, Huang DP. Ultrasonographic findings of triple-negative breast cancer. *Int J Clin Exp Med*. 2015;8(6):10040-10043.
- Azzam H, Kamal R, El-Assaly H, Metwally LIA. The value of dynamic contrast-enhanced MRI in differentiating triple-negative breast cancer from other subtypes. *Egypt J Radiol Nucl Med*. 2019;50(1):106. [\[CrossRef\]](#)
- Sha YS, Chen JF. MRI-based radiomics for the diagnosis of triple-negative breast cancer: a meta-analysis. *Clin Rad*. 2022;S0009-9260(22):00222-00227. [\[CrossRef\]](#)
- Sohn YM, Han K, Seo M. Immunohistochemical subtypes of breast cancer: correlation with clinicopathological and radiological factors. *Iran J Radiol*. 2016;13(4):e31386. [\[CrossRef\]](#)
- Youk JH, Son EJ, Chung J, Kim JA, Kim EK. Triple-negative invasive breast cancer on dynamic contrast-enhanced and diffusion-weighted MR imaging: comparison with other breast cancer subtypes. *Eur Radiol*. 2012;22(8):1724-1734. [\[CrossRef\]](#)
- Ma M, Liu R, Wen C, et al. Predicting the molecular subtype of breast cancer and identifying interpretable imaging features using machine learning algorithms. *Eur Radiol*. 2022;32(3):1652-1662. [\[CrossRef\]](#)
- Krizmanich-Conniff KM, Paramagul C, Patterson SK, et al. Triple receptor-negative breast cancer: imaging and clinical characteristics. *AJR Am J Roentgenol*. 2012;199(2):458-464. [\[CrossRef\]](#)
- Schrading S, Kuhl CK. Mammographic, US, and MR imaging phenotypes of familial breast cancer. *Radiology*. 2008;246(1):58-70. [\[CrossRef\]](#)
- Grimm LJ, Johnson KS, Marcom PK, Baker JA, Soo MS. Can breast cancer molecular subtype help to select patients for preoperative MR imaging? *Radiology*. 2015;274(2):352-358. [\[CrossRef\]](#)
- Ha R, Jin B, Mango V, et al. Breast cancer molecular subtype as a predictor of the utility of preoperative MRI. *AJR Am J Roentgenol*. 2015;204(6):1354-1360. [\[CrossRef\]](#)
- Kim WH, Han W, Chang JM, Cho N, Park IA, Moon WK. Location of triple-negative breast cancers: comparison with estrogen receptor-positive breast cancers on MR imaging. *PLoS One*. 2015;10(1):e0116344. [\[CrossRef\]](#)

# The Relationship Between Dorsal Subcutaneous Fat Tissue Thickness and Lumbar Disc Herniation: A Magnetic Resonance Imaging-Based Study

Volkan Kızılgöz 

Department of Radiology, Erzincan Binali Yıldırım University, Erzincan, Turkey

**Cite this article as:** Kızılgöz V. The relationship between dorsal subcutaneous fat tissue thickness and lumbar disc herniation: A magnetic resonance imaging-based study. *Current Research in MRI*. 2022; 1(2): 38-41.

**Corresponding author:** Volkan Kızılgöz, e-mail: volkankizilgoz@gmail.com

**Received:** October 1, 2022 **Accepted:** October 26, 2022

DOI:10.5152/CurrResMRI.2022.221832



Content of this journal is licensed under a Creative Commons Attribution-NonCommercial 4.0 International License.

## Abstract

**Objective:** The aim of this study was to find out the relationship between dorsal subcutaneous fat tissue thickness and lumbar disc herniation.

**Methods:** The lumbar magnetic resonance images of 209 were re-interpreted. Of these patients, 107 had disc herniation (herniated group), while 102 of them had no disc herniation (non-herniated group) in lumbar magnetic resonance images. The dorsal subcutaneous fat tissue thickness was measured for each patient on lumbar magnetic resonance imaging and the results were compared between these groups. The dorsal subcutaneous fat tissue thickness was measured on magnetic resonance images at the L4-5 and L5-S1 levels for all the patients included in the study and the measurement results were compared with an independent *t*-test for all groups.

**Results:** There was no statistically significant difference between herniated and non-herniated groups according to the measurement results of the dorsal subcutaneous fat tissue thickness ( $P = .446$ ). No significant differences were observed within different age groups or within females and males either.

**Conclusion:** No relationship was found between dorsal subcutaneous fat tissue thickness and lumbar disc herniations according to the results of this study.

**Keywords:** Disc herniation, adipose tissue, magnetic resonance imaging, lumbosacral region

## INTRODUCTION

Balanced body composition is crucial for health and physical activities. Inactivity and body composition-related chronic diseases are accepted as one of the most important public health problems of the 21st century.<sup>1</sup> Some authors in the literature claimed that increased body weight might have biomechanical effects on lumbar spine alignment.<sup>2</sup> These biomechanical stresses are well known to play a role in vertebral pathologies.<sup>3,4</sup> The alterations of the spinal biomechanics led the authors to investigate the possible relationship between low back pain and body weight.<sup>5</sup> Optimal anatomical alignment of the bones and joints renders an effective function of the musculoskeletal system, and disc herniations are one of the most common problems of the spine, which causes low back pain and decreases the quality of life of the individual. Magnetic resonance (MR) imaging enables the detection of disc pathologies and explains the underlying cause of the radiculopathies with its excellent soft tissue contrast. There are some parameters that were claimed to be related to disc pathologies in the literature. Dorsal subcutaneous fat tissue thickness (DSFTT) is one of the parameters which were studied before using MR images and the investigators tried to find out the relationship between DSFTT, obesity, and disc degeneration.<sup>6,7</sup> This current study aimed to focus on revealing the relationship between lumbar disc herniations and DSFTT which can easily be measured on MR images.

## METHODS

### Patients

This research was designed as a retrospective cross-sectional study. After the approval of this study by the institutional ethics committee (Ethics Committee of Erzincan Binali, Yıldırım University, Date: 02.11.2022, Session: 04, Number: E-26447783-050.06.04-212526), the lumbar MR images of 345 patients who had undergone MR examination between January 1, 2022, and January 20, 2022, have been re-interpreted. The patients who had any disc herniation (disc protrusion or extrusion) in L4-5 or L5-S1 or both these intervertebral disc levels were chosen as the “herniated” group. The patients who had no disc herniations in any intervertebral disc levels were chosen as the “non-herniated” group and disc bulging was also included in this category since this pathology is not accepted as a real disc herniation. Patients with any previous lumbar spinal surgery, congenital anomalies, scoliosis, vertebral deformities, or malignant lesions on MR images were excluded. Since this study aimed to investigate the relationship between DSFTT and lumbar disc herniations in skeletally mature individuals, patients under 18 years old were excluded. As a result, 209 MR images, each belonging to a different patient were considered to calculate the statistical results.



### Lumbar Magnetic Resonance Imaging and Interpretation

Magnetic resonance imaging for the lumbar region was handled by a standard protocol used for disc pathologies. All MR images were obtained by a 1.5 T MR machine (Magnetom Aera, Siemens, Erlangen, Germany) and with 32-channel lumbar coils. The patients were in the supine position in the MR machine while the images were acquired. Sagittal plane T2-weighted images (TR [Time of Repetition]: 4120 ms, TE [Time of Echo]: 104 ms, average: 2, field of view: 280 mm, slice thickness: 4 mm, voxel size:  $0.9 \times 0.9 \times 4$  mm), sagittal plane T1-weighted images (TR: 646 ms, TE: 9 ms, average: 2, field of view: 280 mm, slice thickness: 4 mm, voxel size:  $0.9 \times 0.9 \times 4$  mm), and axial plane T2-weighted images (TR: 5070 ms, TE: 88 ms, average: 1, field of view: 190 mm, slice thickness: 4 mm, voxel size:  $0.7 \times 0.7 \times 4$  mm) were obtained from each patient as a part of a routine lumbar spinal study with regard to intervertebral disc protocols. All MR images were re-evaluated by a radiologist with 17 years of experience. A picture archiving and communication system (Akgün PACS Viewer v7.5, Akgün Software, Ankara, Turkey) was used to analyze the MR images and make measurements in standard digital imaging and medicine formats.

### Dorsal Subcutaneous Fat Tissue Thickness Measurement and Statistical Analysis

The DSFTT measurements were done on MR images at the L4-5 and L5-S1 levels for all the patients included in the study. The thickness of the dorsal subcutaneous fat was measured perpendicularly to the skin surface in mid-sagittal T1-weighted images (Figure 1). The average value of these 2 levels was considered in the statistical calculations. All statistical calculations were achieved using the Statistical Package for the Social Sciences version 22.0. (IBM SPSS Corp.; Armonk, NY, USA). The Kolmogorov–Smirnov test was carried out to find out the distribution characteristics of the data and the association between the DSFTT measurements was compared with an independent *t*-test for all groups. To analyze the test results, *P* values less than .05 were accepted to indicate statistical significance.

### RESULTS

The age and sex distribution of the patients included in this study were shown in Table 1. There was no significant difference between herniated and non-herniated groups with regard to age ( $P = .844$ ). There was no statistically significant difference between herniated and non-herniated groups' DSFTT measurements ( $P = .446$ ).

The data set was also studied to calculate a possible significant difference between age groups (<40 years and  $\geq 40$  years) and any difference between females and males with regard to DSFTT measurement

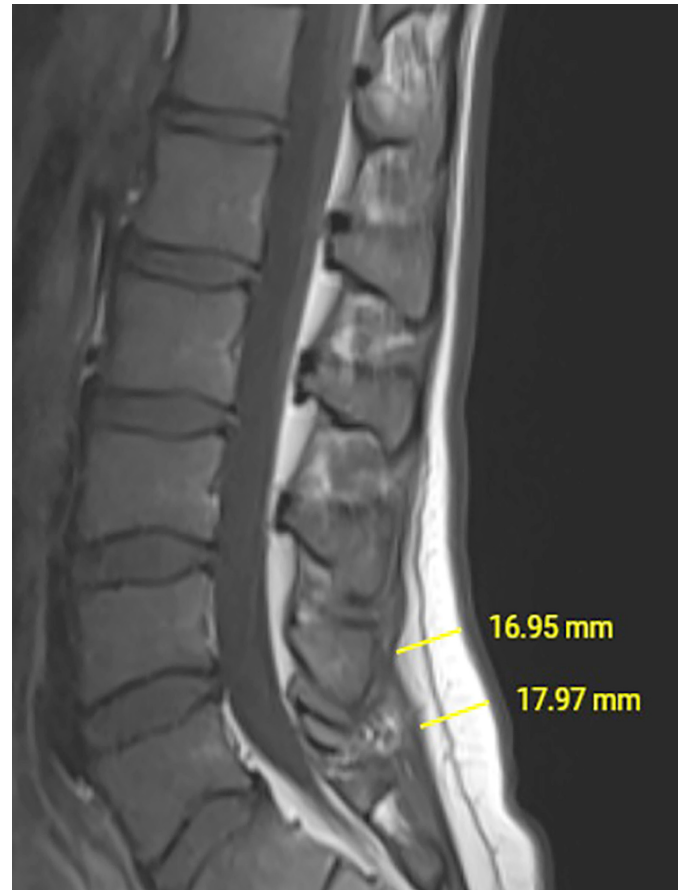


**Figure 1.** The dorsal subcutaneous fat thickness was measured on sagittal T1-weighted images as shown in the figure.

results. The age groups revealed no significant difference, and the mean DSFTT value of the males was significantly lower than females ( $P < .001$ ) (Table 2).

**Table 1.** Age and Sex Distribution of Patients

	Herniated	Non-herniated	<i>P</i>
n	107	102	
Sex (F/M)	65F/42M	60F/42M	
Mean age	43 ± 14	43 ± 13	.844
Mean DSFTT (mm)	26.62 ± 12.96	25.94 ± 14.23	.446

DSFTT, dorsal subcutaneous fat thickness; F, female; M, male.

**Table 2.** Dorsal Subcutaneous Fat Tissue Thickness Measurements Regarding Age and Sex

Age	<40 Years (n=84)	$\geq 40$ Years (n=125)	<i>P</i>
Mean DSFTT (mm)	38.43 ± 27.41	38.60 ± 24.72	.948
Sex	Female (n=125)	Male (n=84)	
Mean DSFTT (mm)	42.67 ± 25.31	32.12 ± 25.18	<b>&lt;.001</b>

The results in bold represents the statistically significant values

**Table 3.** Dorsal Subcutaneous Fat Tissue Thickness Measurements of the Female Group

	n	Mean	Standard Deviation	<i>P</i>
Herniated	65	43.02	25.79	.769
Non-herniated	60	42.08	24.86	

### MAIN POINTS

- Low back pain may cause decreased physical function, compromised life quality, and psychological stress.
- Obesity is recognized as another factor playing a role in low back pain.
- In the literature, there are researchers indicating the association between low back pain and disc degeneration both for adolescents and adults.
- A high correlation between body fat percentage and dorsal subcutaneous fat tissue thickness was shown by some investigators.
- The results of this current study indicated no relationship between dorsal subcutaneous fat tissue thickness and intervertebral disc herniations



**Table 4.** Dorsal Subcutaneous Fat Tissue Thickness Measurements of the Male Group

	n	Mean	Standard deviation	P
Herniated	42	33.31	26.04	.420
Non-herniated	42	30.20	23.56	

**Table 5.** Dorsal Subcutaneous Fat Tissue Thickness Measurements of the Group Younger Than 40 Years

	n	Mean	Standard Deviation	P
Herniated	45	41.74	28.32	.074
Non-herniated	39	34.10	25.81	

**Table 6.** Dorsal Subcutaneous Fat Tissue Thickness Measurements of the 40 Years and Older Group

	n	Mean	Standard Deviation	P
Herniated	62	37.45	24.64	.553
Non-herniated	63	39.30	24.47	

The difference between herniated and non-herniated groups was also calculated within each gender group and both indicated no significant difference (Tables 3 and 4). There was no difference between the patients younger than 40 years (Table 5) and 40 years or older (Table 6) either.

## DISCUSSION

Low back pain may cause decreased physical function, compromised life quality, and psychological stress.<sup>8</sup> Obesity is recognized as another factor playing a role in low back pain.<sup>9,10</sup> In the literature, there are researchers indicating the association between low back pain and disc degeneration both for adolescents<sup>11</sup> and adults.<sup>12</sup> A high correlation between body fat percentage and DSFTT was shown by some investigators.<sup>7</sup> Koda et al<sup>13</sup> used sonography and MR imaging together to measure the correlation between sonographic fat tissue thickness and visceral fat volume. They have found an association between sonographic subcutaneous fat index (fat thickness at the umbilicus level/height) and subcutaneous fat thickness were significantly correlated with subcutaneous fat volume measured on MR imaging. Another study in the literature indicated that subcutaneous fat tissue thickness at upper lumbar levels has been found to predict severe intervertebral disc degeneration and Modic changes better than body mass index.<sup>14</sup> Endorsed from all these data and associations underlined by the researchers in the literature, this current study tried to find out the possible relationship between lumbar disc hernias and DSFTT; however, the results showed no relationship between DSFTT and lumbar disc herniation.

Due to the mobility of the lumbosacral part of the spine, this segment is known to be prone to disc herniations. Previous literature has indicated that the 75% of lumbar flexion occurs at the lumbosacral joint and 15-20% of flexion occurs at the L4–L5 level.<sup>15</sup> In this study, L4–L5 and L5–S1 intervertebral disc levels were used to analyze since a majority (90-95%) of clinically significant compressive radiculopathies are known to be encountered at these levels.<sup>16</sup>

The study by Okan and Beyhan<sup>17</sup> indicated higher DSFTT values in females than in males. In another study, in which the association between the body mass index of 149 individuals and lumbar adipose tissue thickness was evaluated, women's adipose tissue thickness was

higher than that of men.<sup>18</sup> The results in this current study were similar to these investigations in the literature. In women, estrogen receptors are more common and there are fewer androgen receptors in subcutaneous adipose tissue. On the other hand, androgen receptors are more predominant in visceral adipose tissue in men.<sup>19</sup> Some authors explained higher DSFTT values in women and claimed that higher subcutaneous adipose tissue thickness in women may be a result of a higher prevalence of estrogen receptors in subcutaneous adipose tissue compared to men.<sup>17</sup>

There are some limitations of this study to discuss. First, to better understand the effect of the amount of axial force on the spine, body mass index should be verified for each patient and the relationship between DSFTT and body mass index should also be studied to analyze the risk factors of the patients for lumbar disc herniation; however, this study focused on a direct relationship between disc herniations and DSFTT. Second, all measurements were done by 1 radiologist. It would be a lot better to measure the DSFTT with more than 1 reviewer and calculate the intra- and interobserver differences. In addition, disc herniations were decided by MR images and the herniated group was planned on the radiological evidence. Re-evaluating the preoperative MR images of the patients that are known to have undergone lumbar disc surgery would be better to compare the measurements with the non-herniated group to support the accuracy of the results of the study. Despite the limitations, there were also opportunities to increase the accuracy of the results of this study. In general, lumbar disc herniations tend to increase through aging. Despite this fact, the insignificance of the age difference between the herniated and non-herniated groups in this investigation rendered a better comparison of the statistical results between these groups.

## CONCLUSION

Dorsal subcutaneous fat tissue thickness is easy to measure on MR images. This parameter is mentioned to be related to obesity and disc degeneration in the literature. However, the results of this study indicated no relationship between DSFTT and intervertebral disc herniations. More studies with larger patient groups are needed to show or rule out this relationship in the literature.

**Ethics Committee Approval:** This study has been approved by the institutional Ethics Committee of Erzincan Binali Yıldırım University, Faculty of Medicine (Date October 13, 2022, Decision No: EBYUKAEK- E-352 78931 0-040 .00.0 2-187 432).

**Informed Consent:** The ethics committee has waived the informed consent from each patient due to the methodology of the study.

**Peer-review:** Externally peer-reviewed.

**Declaration of Interests:** The authors have no conflicts of interest to declare.

**Funding:** The authors declared that this study has received no financial support.

## REFERENCES

1. Blair SN. Physical inactivity: the biggest public health problem of the 21st century. *Br J Sports Med.* 2009;43(1):1-2.
2. Onyemaechi NO, Anyanwu GE, Obikili EN, Onwuasoigwe O, Nwankwo OE. Impact of overweight and obesity on the musculoskeletal system using lumbosacral angles. *Patient Prefer Adherence.* 2016;10:291-296. [CrossRef]
3. Barrey C, Jund J, Nosedà O, Roussouly P. Sagittal balance of the pelvis-spine complex and lumbar degenerative diseases. A comparative study about 85 cases. *Eur Spine J.* 2007;16(9):1459-1467. [CrossRef]

4. Funao H, Tsuji T, Hosogane N, et al. Comparative study of spinopelvic sagittal alignment between patients with and without degenerative spondylolisthesis. *Eur Spine J*. 2012;21(11):2181-2187. [\[CrossRef\]](#)
5. Sheng B, Feng C, Zhang D, Spitler H, Shi L. Associations between obesity and spinal diseases: a medical expenditure panel study analysis. *Int J Environ Res Public Health*. 2017;14(2):183. [\[CrossRef\]](#)
6. Berikol G, Ekşi MŞ, Aydın L, Börekci A, Özcan-Ekşi EE. Subcutaneous fat index: a reliable tool for lumbar spine studies. *Eur Radiol*. 2022;32(9):6504-6513. [\[CrossRef\]](#)
7. Takatalo J, Karppinen J, Taimela S, et al. Association of abdominal obesity with lumbar disc degeneration--a magnetic resonance imaging study. *PLoS One*. 2013;8(2):e56244. [\[CrossRef\]](#)
8. Deyo RA, Mirza SK, Martin BI. Back pain prevalence and visit rates: estimates from U.S. national surveys, 2002. *Spine (Phila Pa 1976)*. 2006;31(23):2724-2727. [\[CrossRef\]](#)
9. Urquhart DM, Berry P, Wluka AE, et al. 2011 Young Investigator Award Winner: increased fat mass is associated with high levels of low back pain intensity and disability. *Spine (Phila Pa 1976)*. 2011;36(16):1320-1325. [\[CrossRef\]](#)
10. Shiri R, Karppinen J, Leino-Arjas P, Solovieva S, Viikari-Juntura E. The association between obesity and low back pain: a meta-analysis. *Am J Epidemiol*. 2010;171(2):135-154. [\[CrossRef\]](#)
11. Samartzis D, Karppinen J, Mok F, Fong DY, Luk KD, Cheung KM. A population-based study of juvenile disc degeneration and its association with overweight and obesity, low back pain, and diminished functional status. *J Bone Joint Surg Am*. 2011;93(7):662-670. [\[CrossRef\]](#)
12. Cheung KMC, Karppinen J, Chan D, et al. Prevalence and pattern of lumbar magnetic resonance imaging changes in a population study of one thousand forty-three individuals. *Spine*. 2009;34(9):934-940. [\[CrossRef\]](#)
13. Koda M, Senda M, Kamba M, Kimura K, Murawaki Y. Sonographic subcutaneous and visceral fat indices represent the distribution of body fat volume. *Abdom Imaging*. 2007;32(3):387-392. [\[CrossRef\]](#)
14. Özcan-Ekşi EE, Kara M, Berikol G, Orhun Ö, Turgut VU, Ekşi MŞ. A new radiological index for the assessment of higher body fat status and lumbar spine degeneration. *Skelet Radiol*. 2022;51(6) :1261-1271. [\[CrossRef\]](#)
15. Alter MJ. *Science of Flexibility*. 3rd ed, Champaign: HumanKinetics; 2004:239.
16. Deyo RA, Weinstein JN. Low back pain. *N Engl J Med*. 2001;344(5):363-370. [\[CrossRef\]](#)
17. Okan S, Beyhan M. Relationship between lumbar subcutaneous adipose tissue thickness and spinopelvic parameters. *Cukurova Med J*. 2020;45(3):1238-1245. [\[CrossRef\]](#)
18. West W, Brady-West D, West KP. A comparison of statistical associations between oedema in the lumbar fat on MRI, BMI and back fat thickness (BFT). *Heliyon*. 2018;4(1):e00500. [\[CrossRef\]](#)
19. Chang E, Varghese M, Singer K. Gender and sex differences in adipose tissue. *Curr Diabetes Rep*. 2018;18(9):69. [\[CrossRef\]](#)

# Is Fusion Imaging Mandatory to Detect the Localization of Middle Ear Cholesteatomas? Inter-rater Reliability in Assessment

Umut Perçem Orhan Söylemez<sup>1</sup> , Başak Atalay<sup>2</sup> , Nesrin Gündüz<sup>2</sup> , Sabriye Gülçin Bozbeyoğlu<sup>1</sup> , Ali Fırat<sup>2</sup> 

<sup>1</sup>Department of Radiology, Prof. Dr.Süleyman Yalçın Göztepe City Hospital, İstanbul, Turkey

<sup>2</sup>Department of Radiology, İstanbul Medeniyet University, Faculty of Medicine, İstanbul, Turkey

**Cite this article as:** Perçem Orhan Söylemez U, Atalay B, Gündüz N, Gülçin Bozbeyoğlu S, Fırat A. Is fusion imaging mandatory to detect the localization of middle ear cholesteatomas? Inter-rater reliability in assessment. *Current Research in MRI*. 2022; 1(2): 42-46.

This study was presented as oral scientific presentation in Turkish Society of Neuroradiology 31st Annual Meeting, Istanbul 2022.

**Corresponding author:** Umut Perçem Orhan Söylemez, e-mail: umutpercem@gmail.com

**Received:** July 24, 2022 **Accepted:** September 16, 2022

DOI: 10.5152/CurrResMRI.2022.221627



Content of this journal is licensed under a Creative Commons Attribution-NonCommercial 4.0 International License.

## Abstract

**Objective:** Non-echo planar diffusion-weighted imaging sequence and fusion imaging are increasingly used in the diagnosis of cholesteatoma. But it is still challenging to locate cholesteatomas and differentiate from other opacifications. This study aimed to evaluate whether the exact localization of cholesteatomas could be detected without fusion imaging using diffusion and T2-weighted magnetic resonance images in combination with computed tomography.

**Methods:** The study included patients with a diagnosis of cholesteatoma and had both temporal bone magnetic resonance imaging and computed tomography between 2017 and 2021. Presence of cholesteatomas was confirmed in non-echoplanar diffusion-weighted images prior to evaluation. Then, the localization of the lesion on computed tomography image was classified by detecting the equivalent of the lesion on T2-weighted thin-sliced images. All images were assessed by 2 independent radiologists. Kappa correlation coefficient was used to evaluate the interobserver agreement.

**Results:** Eighty-nine patients (49 female, 40 male) were included. The mean age was 39.07 (5-89). Interobserver agreement was moderate to almost perfect according to localization of cholesteatomas. The  $\kappa$  coefficient ranged between 0.48 and 0.83. The highest agreement was detected for the lesions located in the mesotympanium ( $\kappa=0.83$ ), external acoustic canal, and mastoid bone. However, a moderate agreement was detected for lesions located in the medial epitympanic recess ( $\kappa=0.49$ ).

**Conclusion:** Cholesteatomas which are placed in the mesotympanium, external auditory canal, and mastoid bone can be determined with high accuracy without fusion imaging.

**Keywords:** Tomography, diffusion, temporal bone, cholesteatoma

## INTRODUCTION

Cholesteatomas are defined as the appearance of skin tissue in the inappropriate localizations; they are well-circumscribed non-neoplastic lesions observed in the temporal bone.<sup>1</sup> Middle ear cholesteatomas are common pathologies seen as a complication of untreated chronic otitis media, especially in underdeveloped countries.<sup>2</sup> While very small cholesteatomas can be detected with non-echo planar diffusion-weighted imaging (non-EPI DWI), anatomical details cannot be distinguished. Thin-section computed tomography (CT) provides excellent information on anatomical details.<sup>2</sup> Therefore, both CT and magnetic resonance imaging (MRI) are generally used in combination.

Diffusion-weighted imaging plays an important role in distinguishing cholesteatomas from other secretions, granulation tissue, scar tissue, and encephalocele.<sup>3</sup> Non-echo planar diffusion-weighted imaging, which is less affected by susceptibility artifacts, has high sensitivity (91%) and specificity (96%) in detecting cholesteatoma. Non-echo planar diffusion-weighted imaging sequence is superior to EPI DWI sequences in detecting the presence of cholesteatoma and has a higher positive predictive value. Therefore, it is recommended that it should be standardized in cholesteatoma imaging. However, its anatomical resolution is insufficient in a very small area such as the temporal bone.<sup>3</sup> At that point, thin-section high-resolution temporal bone CT becomes important. But, CT is still insufficient to distinguish cholesteatomas from other fluids and tissues.<sup>3</sup> On the other hand, MRI has the advantage of showing extension into the membranous labyrinth in some cases of cholesteatomas.<sup>3</sup> Therefore, fusion imaging combining CT and MRI has been the subject of study in recent years and has begun to be used.<sup>4,5</sup> However, fusion imaging has several limitations: it is cumbersome and requires the use of 2 different imaging modalities per patient. In this study, we aimed to classify cholesteatomas into anatomical groups by evaluating thin-sliced T2-weighted images and non-EPI DWI and CT scans together and to evaluate the reliability of localization of the lesions among observers.

## METHODS

Prior to this retrospective study, approval was obtained from the university ethics committee. (ID: 2021/0496, date: 10/6/2021). Only patients having both thin-sliced temporal bone CT and temporal bone MRI were included to the study. Images with artefacts, without non-EPI DWI, and thin-section T2 sequences, without thin-section temporal bone scans, were excluded. Two independent observers (with 10 years of experience in neuroradiology and 5 years of experience in head and neck radiology) evaluated non-EPI DWI, thin-sliced T2, and thin-sliced CT images for all patients to classify localization of the cholesteatomas.

### Imaging Technique and Diagnosis

For temporal bone CT, acquisition parameters were as follows: 100 mAs, 100 kV, 0.6 s rotation time, 1 mm/rotation (pitch, 0.984), 0.625 mm slice thickness, 2.8 s scan time, field of view of 200 mm and matrix of  $512 \times 512$ .

For temporal bone MRI, T1- and T2-weighted sequences with a 3 mm slice thickness, 3D-FIESTA sequence with 0.5 mm slice thickness, fluid-attenuated inversion recovery, and non-EPI diffusion-weighted sequence (b-value:  $1000 \text{ s/mm}^2$ ) were achieved.

Localizations of cholesteatomas were described as external auditory canal, mastoid bone, periossicular chain, medial, lateral or superior epitympanic recess, mesotympanium, hypotympanium, Prussak's space, pars tensa, and pars flaccida (Figure 1). The localization, which was restricted in favor of cholesteatoma in diffusion MRI, was determined in thin-section T2 images, and its localization in the CT image was decided and detailed anatomically (Figures 2, 3, 4).

### Statistical Analysis

The Statistical Package for the Social Sciences version 19.0. (IBM SPSS Corp.; Armonk, NY, USA). Quantitative data were interpreted using means and SDs and minimum and maximum values. Qualitative data were interpreted using frequencies, percentages, and ranges. Interobserver agreement assessed was based on the kappa coefficient ( $\kappa$ ).  $\kappa \leq 0$  is defined as no agreement, between 0.01 and 0.20 as none to slight, between 0.21 and 0.40 as fair, between 0.41 and 0.60 as moderate, between 0.61 and 0.80 as substantial, and between 0.81 and 1.00 as almost perfect agreement.<sup>6</sup>

## RESULTS

One hundred thirty medical records were assessed. After initial evaluation, 89 patients [49 (55.05%) female, 40 (44.9%) male] with cholesteatoma were included the study. All cases were unilateral. There were 44 right- and 45 left-sided cholesteatomas. The mean age was  $39.0 \pm 62.2$  (5-89). The most common localization was periossicular chain ( $n=37$ , 41.5%) and attic cavity superior ( $n=26$ , 29.2%) and the less common localization was lateral epitympanic recess ( $n=9$ , 10.1%). The hearing loss was noted for 60 patients and facial paralysis for only 1 patient. Twenty-eight patients had residual recurrent cholesteatoma in the mastoidectomy cavity, and these lesions were detected with almost perfect interobserver agreement ( $\kappa=0.81$ ).

According to kappa correlation coefficient, interobserver agreement changed between almost perfect and moderate agreement. The kappa correlation coefficient was between 0.48 and 0.83 (Table 1).

## DISCUSSION

In this study, the localization of cholesteatomas was divided into anatomical subgroups and evaluated with CT and MR images; the highest agreement was detected for the lesions located in the mesotympanium ( $\kappa=0.83$ ), external acoustic canal ( $\kappa=0.81$ ), and mastoid bone ( $\kappa=0.80$ -0.81). However, a moderate agreement was detected for lesions located in the medial epitympanic recess ( $\kappa=0.49$ ) and Prussak's space ( $\kappa=0.51$ ).

Non-echo planar diffusion-weighted imaging is very sensitive even for detecting very small cholesteatomas.<sup>7</sup> Especially for residual or recurrent cholesteatoma, non-EPI DWI parameters are more reliable (91% sensitivity and 96% specificity), but CT is perfect for anatomic detail.<sup>2,8</sup> Therefore, fusion studies were carried out with the idea of benefiting from the advantages of CT and MRI together. Few studies with a small patient group reported that fusion imaging is better than only CT or only MRI.<sup>4,9</sup> Fusion software is costly and time consuming. Moreover, it is not accessible at every center.<sup>10</sup> Fusion imaging studies are experimental level studies with a small patient group in the form of case series.<sup>10</sup> In studies conducted with a single observer, reliability was not evaluated due to interobserver agreement.<sup>11</sup> The current study aimed to investigate how reliably we could detect cholesteatomas without using fusion imaging with a larger patient group.

Some fusion studies focused on evaluating the presence of cholesteatoma. In these studies, the authors did not make a classification according to lesion localization.<sup>4,5</sup> But cholesteatoma localization is extremely important for surgical planning. There are many guidelines for classifying and staging cholesteatomas.<sup>12</sup> Radiological evaluation is very important to be able to do this before surgery and to guide surgical treatment. Therefore, in the current study, we focused on locating the cholesteatoma rather than detecting its presence.

Plouin-Gaudon et al<sup>13</sup> classified cholesteatoma localizations as hypotympanium, epitympanium, mastoid recess, and attical space in their CT-DWI fusion study with 10 children. However, we performed a more detailed examination with a larger patient cohort (89 patients and 13 different localizations). The number of patients, the evaluation of 2 observers, and the anatomical detailing increased the reliability of the current study.

Alzahrani et al<sup>14</sup> compared the results of CT-DWI fusion imaging and second-look surgery in 10 patients with residual cholesteatoma and recommended fusion imaging for the detection of residual cholesteatomas.

## MAIN POINTS

- While very small cholesteatomas can be detected with non-echo planar diffusion-weighted imaging (non-EPI DWI), anatomical details cannot be distinguished. Thin-section computed tomography (CT) provides excellent information on anatomical details.
- Fusion imaging, combining CT and magnetic resonance imaging (MRI), has been the subject of studies in recent years and has begun to be used.
- Fusion software is costly and time consuming. Moreover, it is not accessible at every center.
- Combined evaluation of high-resolution CT, non-EPI DWI, and T2-weighted MR can detect not only the presence of cholesteatoma but also its localization with high accuracy, even without the need for fusion images for many cholesteatomas.



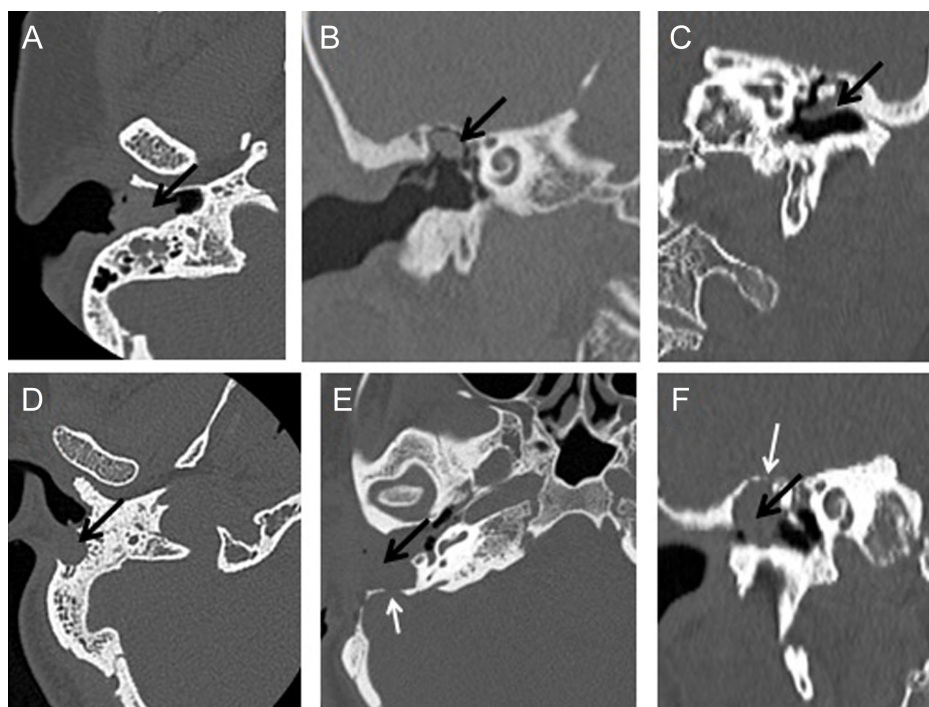


**Figure 1.** The localization definition examples in temporal bone CT images. (A) Right-sided cholesteatoma in external auditory canal (arrow). (B) Right-sided cholesteatoma in superior attic recess (arrow). (C) Left-sided pars flaccida cholesteatoma (arrow). (D) Right-sided mastoid air cell cholesteatoma with bony erosion (arrow). (E) Right-sided cholesteatoma in mastoidectomy cavity (black arrow) and bony erosion in the occipital bone (white arrow). (F) Right-sided cholesteatoma originating from the lateral epitympanic recess and extending into the external auditory canal (black arrow) and bony destruction in the tegmen tympani (white arrow). CT, computed tomography.

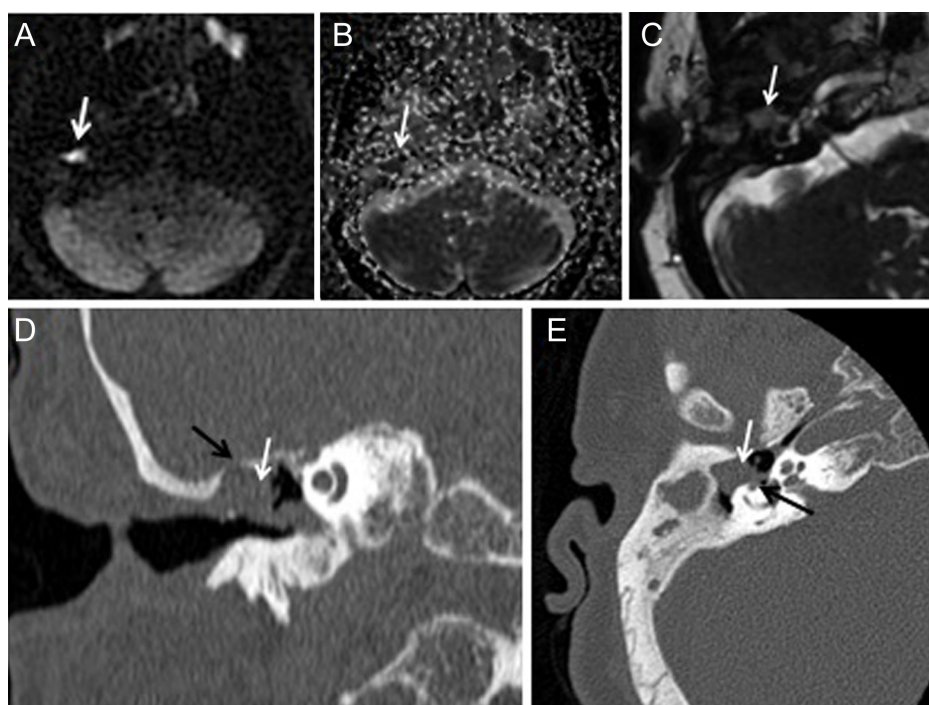


**Figure 2.** Right-sided millimetric nodular diffusion restriction non-echo planar diffusion-weighted image (A) and apparent diffusion coefficient map (B). (C) On thin-sliced T2-weighted image, the nodular lesion in tympanic cavity, fistulized to inner ear. (D) On coronal CT image, the opacity filling the tympanic cavity (white arrow) which is not all cholesteatoma when confirmed by MRI and bony destruction in tegmen tympani (black arrow). (E) Cholesteatoma located in the medial epitympanic recess (white arrow) fistulized into the semicircular canal (black arrow) in the axial CT image corresponding to the thin-section T2-weighted MR image. CT, computed tomography; MRI, magnetic resonance imaging.

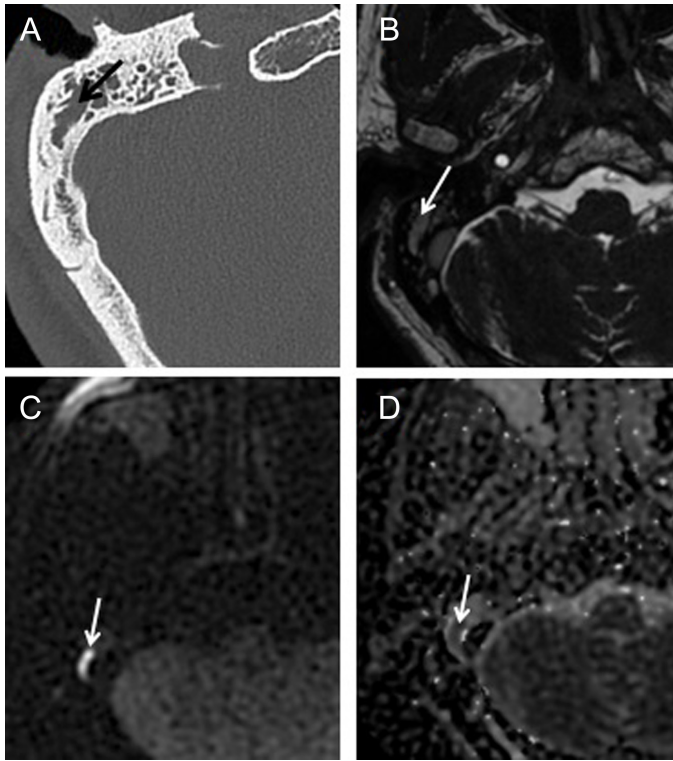


**Figure 3.** (A) In the axial CT image, opacifications (arrow) within the mastoid air cells on the right; it is difficult to distinguish cholesteatoma from other secretions with only CT. (B) Thin-sliced T2-weighted MR image shows hypointense secretions (arrow). (C, D) Fusiform-shaped diffusion restriction in this area (arrows) compatible with cholesteatoma. CT, computed tomography; MR, magnetic resonance.

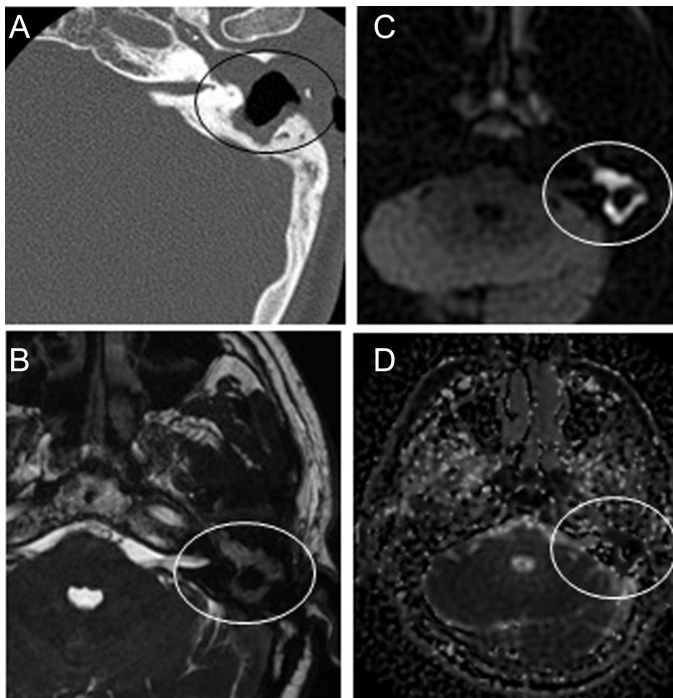


**Figure 4.** (A) Axial CT image, (B) T2-weighted thin-sliced image shows secretions in the same form as C, D. (C, D) Diffusion restriction (rings). CT, computed tomography.

**Table 1.** Interobserver Agreement According to Cholesteatoma Localizations

Cholesteatoma localization	$\kappa$
External auditory canal	0.81
Mastoid air cell	0.80
Mastoid antrum	0.80
Mastoidectomy cavity	0.81
Periosteal chain	0.76
Attic superior	0.66
Medial epitympanic recess	0.48
Lateral epitympanic recess	0.63
Prussak's space	0.51
Pars tensa	0.67
Pars flaccida	0.72
Mesotympanum	0.83
Hypotympanum	0.79

$\kappa$ , kappa correlation coefficient.

In the current study, residual cholesteatoma was detected in 28 patients with high accuracy (almost perfect agreement,  $\kappa=0.81$ ) without the need of fusion imaging.

Benson et al<sup>3</sup> reported a fusion study using thin-section T2-weighted and diffusion sequences instead of fusion studies that always used CT and diffusion MR images. The authors aimed to remove CT necessity especially in postoperative and pediatric patients. The authors compared the surgical results with the evaluation of a single neuroradiologist. The accuracies of unfused DWI and fused DWI-T2 were reported as 76% and 82%, respectively.<sup>3</sup> In the current study, all images were evaluated by 2 experienced radiologist, and also CT-DWI-T2 images were evaluated in addition to single CT-DWI or T2-DWI fusion studies. The exact localization of the cholesteatoma was detected by cross-tabulating the T2 sequence with DWI instead of fusion imaging. Anatomical details confirmed this localization with CT.

To the best of our knowledge, this is the only study in which interobserver agreement was evaluated for the largest number of localizations for cholesteatoma. The lack of comparison with surgical results is a limitation of the study.

In conclusion, combined evaluation of high-resolution CT, non-EPI DWI, and T2 weighted MRI can detect not only the presence of cholesteatoma but also its localization with high accuracy, even without the need for fusion images for many cholesteatomas. However, fusion imaging may be essential for cholesteatomas placed in medial epitympanic recess and Prussak's space.

**Ethics Committee Approval:** Ethics committee approval was received for this study from the ethics committee of Istanbul Medeniyet University (Date: June 10, 2021, Decision No: 2021/0496).

**Informed Consent:** Written informed consent was obtained from all participants who participated in this study.

**Peer-review:** Externally peer-reviewed.

**Author Contributions:** Concept – U.P.O.S.; Design – U.P.O.S., B.A.; Supervision – A.F.; Resources – S.G.B.; Materials – N.G.; Data Collection and/or Processing – U.P.O.S., B.A.; Analysis and/or Interpretation – N.G.; Literature Search – S.G.B.; Writing Manuscript – U.P.O.S.; Critical Review – A.F.

**Declaration of Interests:** The authors have no conflicts of interest to declare.

**Funding:** The authors declared that this study has received no financial support.

## REFERENCES

1. Baráth K, Huber AM, Stämpfli P, Varga Z, Kollias S. Neuroradiology of cholesteatomas. *AJNR Am J Neuroradiol.* 2011;32(2):221-229. [\[CrossRef\]](#)
2. Gulati M, Gupta S, Prakash A, Garg A, Dixit R. HRCT imaging of acquired cholesteatoma: a pictorial review. *Insights Imaging.* 2019;10(1):92. [\[CrossRef\]](#)
3. Benson JC, Carlson ML, Yin L, Lane JJ. Cholesteatoma localization using fused diffusion-weighted images and thin-slice T2 weighted images. *Laryngoscope.* 2021;131(5):E1662-E1667. [\[CrossRef\]](#)
4. Locketz GD, Li PM, Fischbein NJ, Holdsworth SJ, Blevins NH. Fusion of computed tomography and PROPELLER diffusion-weighted magnetic resonance imaging for the detection and localization of middle ear cholesteatoma. *JAMA Otolaryngol Head Neck Surg.* 2016;142(10):947-953. [\[CrossRef\]](#)
5. Yamashita K, Hiwatashi A, Togao O, et al. High-resolution three-dimensional diffusion-weighted MRI/CT image data fusion for cholesteatoma surgical planning: a feasibility study. *Eur Arch Otorhinolaryngol.* 2015;272(12):3821-3824. [\[CrossRef\]](#)
6. McHugh ML. Interrater reliability: the kappa statistic. *Biochem Med.* 2012;22(3):276-282. [\[CrossRef\]](#)
7. Dudau C, Draper A, Gkagkanasiou M, Charles-Edwards G, Pai I, Connor S. Cholesteatoma: multishot echo-planar vs non echo-planar diffusion-weighted MRI for the prediction of middle ear and mastoid cholesteatoma. *BJR Open.* 2019;1(1):20180015. [\[CrossRef\]](#)
8. Jindal M, Riskalla A, Jiang D, Connor S, O'Connor AF. A systematic review of diffusion-weighted magnetic resonance imaging in the assessment of postoperative cholesteatoma. *Otol Neurotol.* 2011;32(8):1243-1249. [\[CrossRef\]](#)
9. Sharma SD, Hall A, Bartley AC, Bassett P, Singh A, Lingam RK. Surgical mapping of middle ear cholesteatoma with fusion of computed tomography and diffusion-weighted magnetic resonance images: diagnostic performance and interobserver agreement. *Int J Pediatr Otorhinolaryngol.* 2020;129:109788. [\[CrossRef\]](#)
10. St Leger D, Singh A, Lingam RK. The utility of computed tomography and diffusion-weighted magnetic resonance imaging fusion in cholesteatoma: illustration with a UK case series. *J Laryngol Otol.* 2020;1-6. [\[CrossRef\]](#)
11. Balik AO, Seneldir L, Verim A, Zer Toros S. The role of fusion technique of computed tomography and non-echo-planar diffusion-weighted imaging in the evaluation of surgical cholesteatoma localization. *Medeni Med J.* 2022;37(1):13-20. [\[CrossRef\]](#)
12. Yung M, Tono T, Olszewska E, et al. EAONO/JOS joint consensus statements on the definitions, classification and staging of middle ear cholesteatoma. *J Int Adv Otol.* 2017;13(1):1-8. [\[CrossRef\]](#)
13. Plouin-Gaudon I, Bossard D, Ayari-Khalfallah S, Froehlich P. Fusion of MRIs and CT scans for surgical treatment of cholesteatoma of the middle ear in children. *Arch Otolaryngol Head Neck Surg.* 2010;136(9):878-883. [\[CrossRef\]](#)
14. Alzahrani M, Alhazmi R, Bélair M, Saliba I. Postoperative diffusion weighted MRI and preoperative CT scan fusion for residual cholesteatoma localization. *Int J Pediatr Otorhinolaryngol.* 2016;90:259-263. [\[CrossRef\]](#)

# Acute Transverse Myelitis in a Child with Down Syndrome After Pfizer-BioNTech COVID-19 Vaccine Second Dose

Esra Sarıgeçili<sup>ID</sup>, Ümit Çelik<sup>ID</sup>, Okan Dilek<sup>ID</sup>, Ulaş Özdemir<sup>ID</sup>

Department of Pediatric Neurology, University of Health Science, Adana City Training and Research Hospital, Adana, Turkey

**Cite this article as:** Sarıgeçili E, Çelik Ü, Dilek O, Özdemir U. Acute transverse myelitis in a child with down syndrome after pfizer-BioNTech COVID-19 vaccine second dose. *Current Research in MRI*. 2022; 1(2): 47-49.

**Corresponding author:** Esra Sarıgeçili, e-mail: sarıgeçiliesra@gmail.com

**Received:** July 21, 2022 **Accepted:** August 19, 2022

DOI: 10.5152/CurrResMRI.2022.220712



Content of this journal is licensed under a Creative Commons Attribution-NonCommercial 4.0 International License.

## Abstract

Many pediatric and adult cases of acute transverse myelitis secondary to COVID-19 infection have been reported in the literature so far, but vaccine-related acute transverse myelitis is very rare. In fact, there have been no reported cases in children until now. Vaccination in children is vital both in the prevention of disease and continuing their social life and education. Hence, we believe that it is essential to follow up and report all of the complications that may occur after vaccination.

**Keywords:** COVID-19, Down syndrome, transverse myelitis, vaccine

## INTRODUCTION

Acute transverse myelitis (ATM) is an inflammatory disease of the spinal cord characterized by rapid onset of motor weakness, sensory alterations, and bladder and bowel dysfunction. Rapid diagnosis and treatment are required.<sup>1</sup> Acute transverse myelitis occurs with parainfectious conditions, demyelinating diseases, spinal cord ischemia, or idiopathic causes. In children, ATM usually occurs after infectious causes, and post-vaccine cases have been reported rarely. Especially in the last 2 years, many ATM cases secondary to severe acute respiratory syndrome coronavirus-2 (SARS-CoV-2) (COVID-19) have been reported in both adults and children during the COVID-19 pandemic. Vaccine-related ATM cases are very rare, even in adults, and no cases have been reported in children so far. The neurological side effects of the post-COVID-19 vaccine are mostly dizziness, headache, pain, muscle spasms, myalgia, and paresthesia, and less frequently are tremor, dysphonia, diplopia, tinnitus, seizures, and the reaction of herpes zoster. Guillain-Barre syndrome (GBS), acute disseminated encephalomyelitis, and ATM have been reported much less frequently in databases.<sup>2</sup>

In this article, a case of ATM, which occurred 15 days after Pfizer-BioNTech COVID-19 vaccine in a pediatric patient with Down syndrome, after immune response has appeared, was reported. We suppose that it is crucial to report all of the complications of the vaccine due to its approval and widespread use in children. In particular, as we learn more about the disease, both disease-related and vaccine-related problems will decrease.

## CASE PRESENTATION

A 17-year-old boy with Down syndrome was admitted to the pediatric emergency service with sudden onset of back and leg pain, inability to walk, and inability to urinate and defecate in the last 24 hours. There was no history of fever, infection, cough, or trauma. The SARS-CoV-2 reverse transcriptase polymerase chain reaction test (rtPCR) from the throat swab was reported to be negative. The Pfizer-BioNTech COVID-19 vaccine had been applied 15 days ago. Medical and family histories were unremarkable. He was conscious, oriented, and cooperative, and his cranial nerves were intact. Deep tendon reflexes were asymmetric positive at the first admission, then were symmetric brisk. Abdominal reflex was positive, muscle strength was 5/5 in the upper extremity, 4/5 in the lower extremity proximal, 2/5 at the left foot, 3/5 at the right foot, the bladder is distended, and globe was positive, and there was no stool sensation (Figure 1). The laboratory examination values were, White blood cell (WBC) 7200 (10<sup>9</sup>/L), Hb 16 (g/dL), thrombocyte 190 000 (10<sup>9</sup>/L). There was no problem with peripheral blood biochemical parameters (Aspartat aminotransferase (AST), Alanine aminotransferase (ALT), urea, creatinine, glucose, uric acid, calcium, and magnesium). Serology for *Borrelia burgdorferi*,

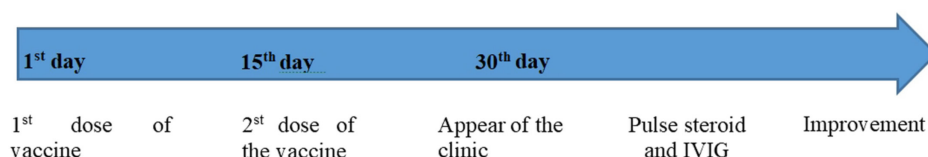


**Figure 1.** Clinical progression of the patient.



**Table 1.** Laboratory Parameters

Parameter	Result	Reference Value
WBC (10 <sup>9</sup> /L)	7200	3.84–9.84
Hgb (g/dL)	16	11–14.5
Platelet (10 <sup>9</sup> /L)	190 000	175 000–332 000
Glucose CSF (mg/dL)	71	40–70
Protein CSF (mg/dL)	42	150–450
Cell CSF (/μL)	-	-
Oligoclonal band CSF	-	-
IgG index CSF	-	-
Glucose serum (mg/dL)	117	60–100
ESR (mm)	14	0–15
CRP (mg/dL)	15	0–5
Vitamin B12 (pg/mL)	106	
ANA	Positive	-
Anti-dsDNA (IU/mL)	Negative	-
C3	0.9	0.79–1.52
C4	0.3	0.16–0.38
Anti-phospholipid ab	0.7	<10
Anti-SSA (AI)	Negative	-
Anti-SSB (AI)	Negative	-
Aquaporin 4 antibody	Negative	-
MOG ab	Negative	-
EBV VCA IgM	0.15	0–0.49
CMV IgM	0.21	0–0.84
Borrelia IgM	1.8	<20

ANA, antinuclear antibody; CRP, C-reactive protein; CSF, cerebrospinal fluid; EBV, Epstein-Barr virus; ESR, Erythrocyte sedimentation rate; SSA, anti-Sjögren's-syndrome-related antigen A; SSB, anti-Sjögren's-syndrome-related antigen B.

cytomegalovirus (CMV), rubella, toxoplasma, Epstein-Barr virus, Herpes simplex virus type 1 and type 2 (HSV-1 and -2) was negative, and also antinuclear antibodies, anti-double-stranded DNA, phospholipid antibodies, cardiolipin antibodies was negative. Vitamin B12 106 (pg/mL) supportive treatment was started. Cerebrospinal fluid analysis was normal for protein, glucose levels, and IgG index; no cells or oligoclonal bands were observed. Serum anti-Myelin oligodendrocyte glycoprotein (MOG) ab, anti-aquaporin 4 (AQP4) ab, and IgG index were all negative (Table 1). Electromyography (EMG) was normal. Contrast-enhanced brain magnetic resonance imaging (MRI) was normal, and there was a signal increase in the cord central extending from L1 and L2 levels to the conus medullaris in spinal MRI (Figure 2). It was evaluated as ATM with the history, clinical, and MRI findings. Methylprednisolone 30 mg/kg/day for 5 days by 20 mg/kg for 2 days, and Intravenous human immunoglobulin (IVIG) 2 g/kg over 5 days were applied, followed by prednisolone 2 mg/kg p.o. His muscle strength, ability to gait, and urination gradually improved. The symptoms appeared on 15th day after the second dose of the vaccine. At first admission, COVID-19 IgG was 28.6 (positive). Since the patient did not have a history of recent infection or trauma, it was primarily considered as a secondary immune reaction to the vaccine.

### MAIN POINTS

- While Infection related Covid-19 diseases are very common, vaccine-related diseases are reported rarely.
- All of the children should be followed up after vaccination.
- Complications should be reported.

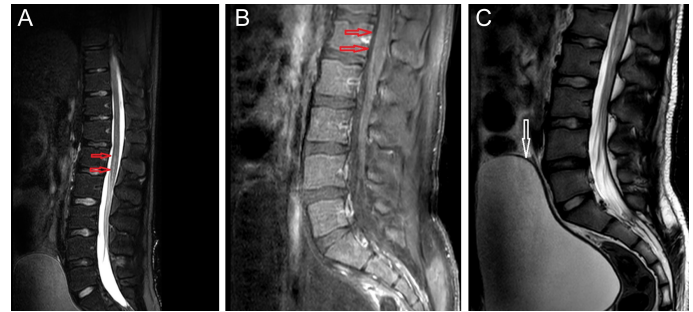


**Figure 2.** Brain and spinal magnetic resonance imaging (MRI) of the patient. (A) Sagittal view of the lumbar spine post-contrast enhancement. T1 shows no contrast enhancement (red arrows). (B) Short T1 inversion recovery (STIR) sagittal view of the lumbar spine shows hyperintensity suggesting demyelination or transverse myelitis in the lower cord and conus medullaris (red arrows). (C) Sagittal T2-weighted lumbar MRI, the bladder is distended (white arrow, globe).

### DISCUSSION

In this article, the first pediatric ATM case that occurred after 15 days after the second dose of Pfizer-BioNTech COVID-19 vaccine, which is an mRNA COVID-19 vaccine, has been reported. Many pediatric and adult cases of ATM secondary to COVID-19 infection have been reported in the literature so far, but vaccine-related ATM is very rare. In fact, there have been no reported cases in children until now. COVID-19-associated ATM may result from abnormal direct or indirect immune pathways, including angiotensin-converting enzyme-2-related pathway, trans-synaptic pathway, hematogenous and lymphatic pathways, or migration of infected immune cells.<sup>3</sup> The COVID-19 pandemic, which was first encountered in 2019, still causes enormous social and economic problems, as well as morbidity and mortality, despite some precautions (such as masks and isolation) taken all over the world.<sup>4,5</sup> It causes morbidity and mortality especially in children even if it does not as much as in adults, apart from educational and social problems. Therefore, it has become crucial for children vaccinated promptly.<sup>6</sup> During the vaccination period, similar to other vaccines (influenza vaccine, hepatitis vaccine, diphtheria-pertussis-tetanus vaccine, polio vaccine), some immune-related problems may be encountered.<sup>7</sup> However, we consider that it is substantial to report complications, especially in children during this common vaccination period. Adult cases of ATM associated with post-vaccination have been reported, so the Pfizer-BioNTech vaccine may be related to a possible disimmunity due to Down syndrome. Albokhari et al<sup>8</sup> reported an ATM case following Pfizer-BioNTech vaccine. Guarnaccia et al<sup>9</sup> reported a case of ATM as the first multiple sclerosis event. At the time of our patient's hospital application, that is 15 days after the second dose of vaccine, the COVID IgG test was positive; this was accepted as an indicator of the immune response to the vaccine. In addition, the absence of any problems in vasculitis parameters, immune parameters, and infectious parameters strongly suggests that there is a secondary immune response to the vaccine in the etiology. We assume that this will be clarified in detail in the following years. However, we believe that the safety, efficacy, immunogenic effects, and dose adjustment of the vaccines used in children should be made according to the clinical and genetic characteristics of the patient. Consequently, vaccination in children is vital both in the prevention of disease and continuing social life and education. Hence, we believe that it is essential to follow up and report all of the complications that may occur after vaccination.

**Informed Consent:** Written informed consent was obtained from all participants who participated in this study.

**Peer-review:** Externally peer-reviewed.

**Author Contributions:** Concept – E.S.; Design – E.S., O.D.; Supervision – U.C.; Data Collection – E.S.; Processing – E.S.; Writing – E.S., U.O.; Critical Review – E.S., O.D.

**Declaration of Interests:** The authors have no conflicts of interest to declare.

**Funding:** The authors declared that this study has received no financial support.

## REFERENCES

1. Krishnan C, Kaplin AI, Pardo CA, Kerr DA, Keswani SC. Demyelinating disorders: update on transverse myelitis. *Curr Neurol Neurosci Rep.* 2006;6(3):236-243. [\[CrossRef\]](#)
2. Goss AL, Samudralwar RD, Das RR, Nath A. ANA investigates: neurological complications of COVID-19 vaccines. *Ann Neurol.* 2021;89(5): 856-857. [\[CrossRef\]](#)
3. Aghagholi G, Gallo Marin B, Katchur NJ, Chaves-Sell F, Asaad WF, Murphy SA. Neurological involvement in COVID-19 and potential mechanisms: a review. *Neurocrit Care.* 2021;34(3):1062-1071. [\[CrossRef\]](#)
4. Zhi ZLXBZ. The epidemiological characteristics of an outbreak of 2019 novel coronavirus diseases (COVID-19) in China. *China CDC Wkly.* 2020;41:145-151.
5. Zhu N, Zhang D, Wang W, et al. A novel coronavirus from patients with pneumonia in China, 2019. *N Engl J Med.* 2020;382(8):727-733. [\[CrossRef\]](#)
6. Kamidani S, Rostad CA, Anderson EJ. COVID-19 vaccine development: a pediatric perspective. *Curr Opin Pediatr.* 2021;33(1):144-151. [\[CrossRef\]](#)
7. Khan E, Shrestha AK, Colantonio MA, Liberio RN, Sriwastava S. Acute transverse myelitis following SARS-CoV-2 vaccination: a case report and review of literature. *J Neurol.* 2022;269(3):1121-1132. [\[CrossRef\]](#)
8. Albokhari AA, Alsawas A, Adnan MH, et al. Acute inflammatory transverse myelitis post-Pfizer-BioNTech-COVID-19 vaccine in 16-year-old. *J Med Res Innov.* 2021;5:47-50. [\[CrossRef\]](#)
9. Guarnaccia J, Creed M, Muriel S. Transverse myelitis as a first event of multiple sclerosis precipitated by Pfizer-BioNTech COVID-19 vaccination. *Neuroimmunol Rep.* 2022;2:100074. [\[CrossRef\]](#)

# Magnetic Resonance Imaging Findings in Osgood Schlatter Disease: A Case Report

Özlem Kadirhan<sup>ID</sup>, Erdem Fatihoğlu<sup>ID</sup>

Department of Radiology, Erzincan University, Faculty of Medicine, Erzincan, Turkey

**Cite this article as:** Kadirhan Ö, Fatihoğlu E. Magnetic Resonance Imaging Findings in Osgood–Schlatter Disease: A Case Report. *Current Research in MRI*. 2022; 1(2): 50-51.

**Corresponding author:** Ozlem Kadirhan, e-mail: ozlemkkadirhan@gmail.com

**Received:** May 5, 2022 **Accepted:** June 19, 2022

DOI:10.5152/CurrResMRI.2022.221015



Content of this journal is licensed under a Creative Commons Attribution-NonCommercial 4.0 International License.

## Abstract

Osgood–Schlatter disease is a tibial tuberosity traction apophysitis caused by recurrent quadriceps femoris muscle tension. It is the most common cause of knee discomfort in children aged 10-15. It is often benign and self-limiting. The stress on the patellar tendon at its point of insertion is the primary cause of this ailment. It is a self-limiting disorder that affects a lot of teenagers. Although our case is similar to the cases reported in the literature, we aimed to present typical magnetic resonance imaging findings.

A 17-year-old male adolescent patient was referred to our clinic because of pain and swelling in the left knee. The patient had knee pain lasting for 10 days. The level of swelling and tenderness was observed in the physical examination. Magnetic resonance imaging examination was performed after a suspicious cortical irregularity was observed on bidirectional knee radiography. In the magnetic resonance imaging examination, we diagnosed the patient with irregular thickening of the tuberositas tibiae and intense edema around it. Non-steroidal anti-inflammatory drugs and rest were recommended to the patient.

Osgood–Schlatter disease is a clinical condition that should be differentiated from many diseases such as avulsion fracture due to the difference in treatment methods.

**Keywords:** adolescent, knee pain, magnetic resonance imaging, Osgood–Schlatter disease, tendinopathy

## INTRODUCTION

Osgood and Schlatter initially described Osgood–Schlatter disease (OSD) in 1903. The patellar tendon's insertion on the skeletally immature tibial tubercle causes OSD, which is a traction phenomenon caused by repetitive quadriceps contraction. In youngsters aged 10-15, it is the most common cause of knee discomfort.<sup>1</sup> It is a disease that affects children. Affected children typically have a history of pain below the patella at the insertion of the patellar tendon, which is exacerbated by sports or other activities such as running or jumping but relieved by rest.<sup>2</sup>

Because of the lack of a specific etiology and thus definition, some physicians may have difficulty distinguishing OSD from tibial tubercle fractures.<sup>3</sup> In this example, patients presented to the emergency department with complaints of knee pain had an OSD that may be mistaken for a fracture.

## CASE PRESENTATION

A 17-year-old male patient, who has been a basketball player for 5 years, applied to the orthopedics clinic with the complaint of left knee pain. It was learned that the patient's pain had been increasing for 10 days. Physical examination revealed swelling and tenderness at the tuberositas tibiae level. Other examinations and laboratory values were normal. We were consulted for a magnetic resonance imaging (MRI) study due to the cortical irregularity seen on the radiograph in the proximal tibia. In the MRI examination, fluid intensity in the suprapatellar bursa and intense edematous signal changes in T2 sequences were observed at the tuberositas tibiae level in the proximal tibia (Figure 1, 2). The patient was recommended non-steroidal anti-inflammatory drug therapy and rest. In the first follow-up after 3 months, there was a significant regression in his pain, except for intense physical activity, and in the second follow-up at 6 months, the pain completely disappeared.

## DISCUSSION

Osgood–Schlatter disease is a benign, self-limiting condition that commonly affects adolescents who participate in sports. Even though OSD is a common occurrence, its consequences are rarely seen because it is a self-limiting disorder. In research by Krause et al<sup>2</sup>, 90% of patients treated with conservative therapy had all of their symptoms resolved within a year of commencement. When the tibial tubercle apophysis ossifies, it normally resolves by the time the patient reaches the age of 18. However, in about 10% of individuals, despite all conservative efforts, the symptoms persist until maturity.<sup>4</sup>

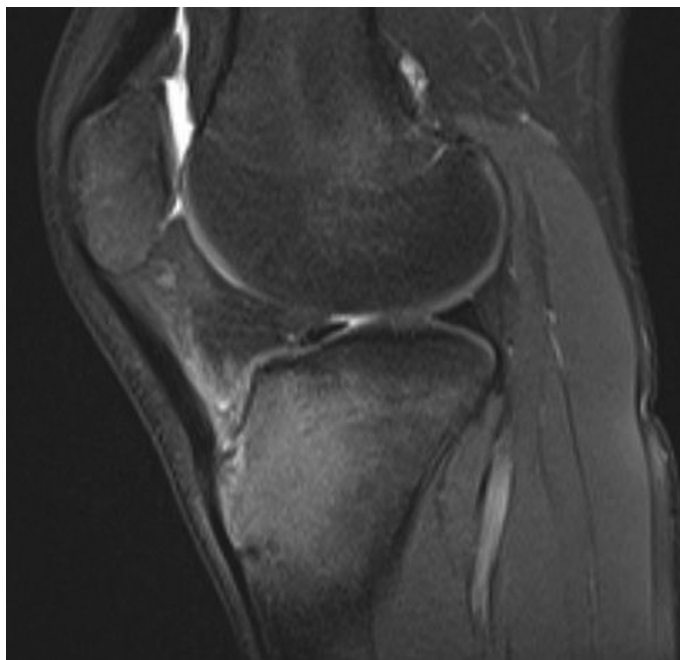


**Figure 1.** In the sagittal T2 image, fluid extending to the suprapatellar plane and bone edema in the tuberositas tibiae were observed.

As in our patient, OSD is more common in boys than girls and usually presents with knee involvement.<sup>5</sup> This is related to the ossification of the tibia. Anamnesis and physical examination are very important to explain the etiology. Patients often complain of pain that increases with exercise. In our case, we saw these complaints in the basketball player.

Radiological findings may be normal, but in most cases, irregularity in the tibial tubercle, patellar tendon thickening, soft tissue swelling around the patellar ligament, and infrapatellar fat pad obliteration can be seen in the lateral radiograph in most cases. In MRI examination, edematous changes can be observed in T2 sequences and irregularities in bone structure can be observed in T1 sequences. Magnetic resonance imaging findings were the same in our case.

Differential diagnosis should include trauma, inflammatory arthropathies such as septic arthritis, rheumatoid arthritis and Reiter's

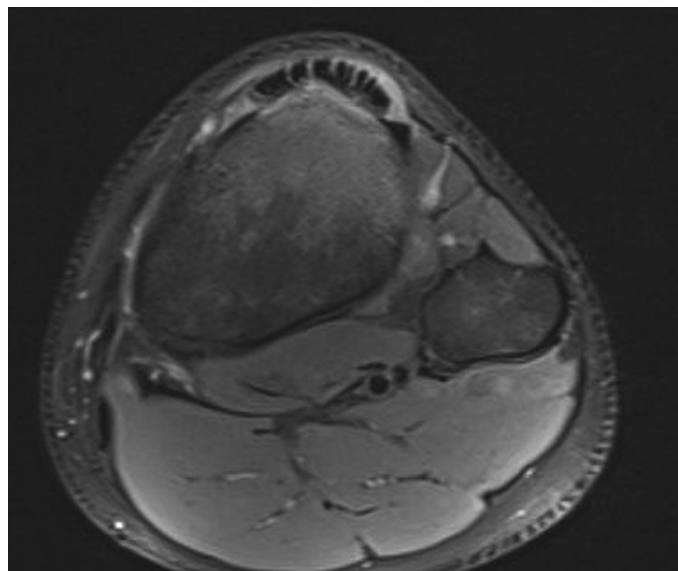


**Figure 2.** Bone edema in tuberositas tibiae and increased cortical thickness in tuberositas tibiae in coronal T2 image.

syndrome, malignancy, patellar subluxation, patellar tendonitis, osteochondritis dissecans, and meniscal diseases. In our patient, we avoided these diagnoses by means of laboratory values, clinical features, and radiological findings and diagnosed OSD. It is usually a self-limiting disease, although it may take several years for the disease to resolve completely. Patients benefit from medical treatment and activity restriction. The place of surgery is very limited. In our case, the pain subsided after 3 months and disappeared after 6 months.

**Peer-review:** Externally peer-reviewed.

**Author Contributions:** Concept – O.K., E.F.; Design – O.K., E.F.; Supervision – O.K., E.F.; Fundings – None; Materials – O.K., E.F.; Data Collection and/or Processing – O.K., E.F.; Analysis and/or Interpretation – O.K., E.F.; Literature Review – O.K., E.F.; Writing – O.K., E.F.; Critical Review Contribution Type – O.K., E.F.

**Declaration of Interests:** The authors have no conflicts of interest to declare.

**Funding:** The authors declared that this study has received no financial support.

## MAIN POINTS

- Osgood–Schlatter disease (OSD) is a tibial tuberosity traction apophysitis caused by repetitive quadriceps femoris muscle tension in adolescents who play sports.
- Although OSD is a common event, its consequences are infrequent as it is a self-limited disorder.
- History and physical examination are very important to explain the etiology. Patients often complain of pain that increases with exercise.
- It may be difficult to distinguish OSD from tibial tubercle fractures by radiography, and at this point, the need to confirm with further examination arises.
- In OSD, edema changes in T2 sequences and irregularities in bone structure can be observed in T1 sequences in magnetic resonance imaging examination.

## REFERENCES

1. Circi E, Atalay Y, Beyzadeoglu T. Treatment of Osgood–Schlatter disease: review of the literature. *Musculoskelet Surg.* 2017;101(3):195-200. [\[CrossRef\]](#)
2. Narayana Gowda BS, Mohan Kumar J. Simultaneous bilateral tibial tubercle avulsion fracture in a case of pre-existing Osgood–Schlatter disease (OSD). *J Orthop Case Rep.* 2012;2(1):24-27.
3. Tulic G, Sopta J, Bumbasirevic M, Todorovic A, Vucetic C. Simultaneous bilateral avulsion fracture of the tibial tubercle in adolescent: a case report. *J Pediatr Orthop B.* 2010;19(1):118-121. [\[CrossRef\]](#)
4. Rathleff MS, Winiarski L, Krommes K, et al. Activity modification and knee strengthening for Osgood–Schlatter disease: a prospective cohort study. *Orthop J Sports Med.* 2020;8(4):2325967120911106. [\[CrossRef\]](#)
5. Gholive PA, Scher DM, Khakharia S, Widmann RF, Green DW. Osgood Schlatter syndrome. *Curr Opin Pediatr.* 2007;19(1):44-50. [\[CrossRef\]](#)